porphyry area located at the southern half of the line. Another small high resistivity zone is present at the northern part from No.2, corresponding with diorite distribution.

Investigation of the resistivity distribution through the plan maps and the pseudo-sections presumes that the zone of apparent low resistivity at the north of survey lines A and B is mostly low resistivity caused by a subterranean flow of water from a mountain peak, and no low resistivity zone caused by mineralization exists because of low PFE values in that area, as will be mentioned later. However the low resistivity zone located along Maden Stream in the south-eastern part of the surveyed area might be caused by both mineralization and underground water.

On the other hand, the high resistivity zone corresponds with andesite lava in the western part, and quartz porphyry in the eastern part of the survey area, and it indicates unaltered rock, considering the results of rock measurement.

(2) Plan Map and Pseudo-Section of Percent Frequency Effect

PFE values in the surveyed area range from -2.8% to 15.5%, having 4.29 % as the arithmetic mean (M). Its values of $M+\sigma$ and $M-\sigma$ are respectively calculated as 7.39 % and 1.19 % using by 3.106 standard deviation (σ). Most rock samples are less than 2 % in PFE value by measurement, except the mudstone. T hus an anomalous PFE value is estimated at over 8 % in the area. A distribution of the PFE anomalous zone is explained as follows .

Plan Map of Percent Frequency Effect

Plan map of n = 1 (Fig. 71)

A PFE anomalous zone over 8 % is located in the area from Line D to Line F of the eastern part of the survey area. Another two small, anomalous PFE zones are also recognized at the western part of Line G. Two PFE areas below 2 % distributed at the northern area and at the area from the central western part to the south-eastern part are presumed to be as unmineralized zones. PFE values tend to become bigger toward the north eastern part of the survey area.

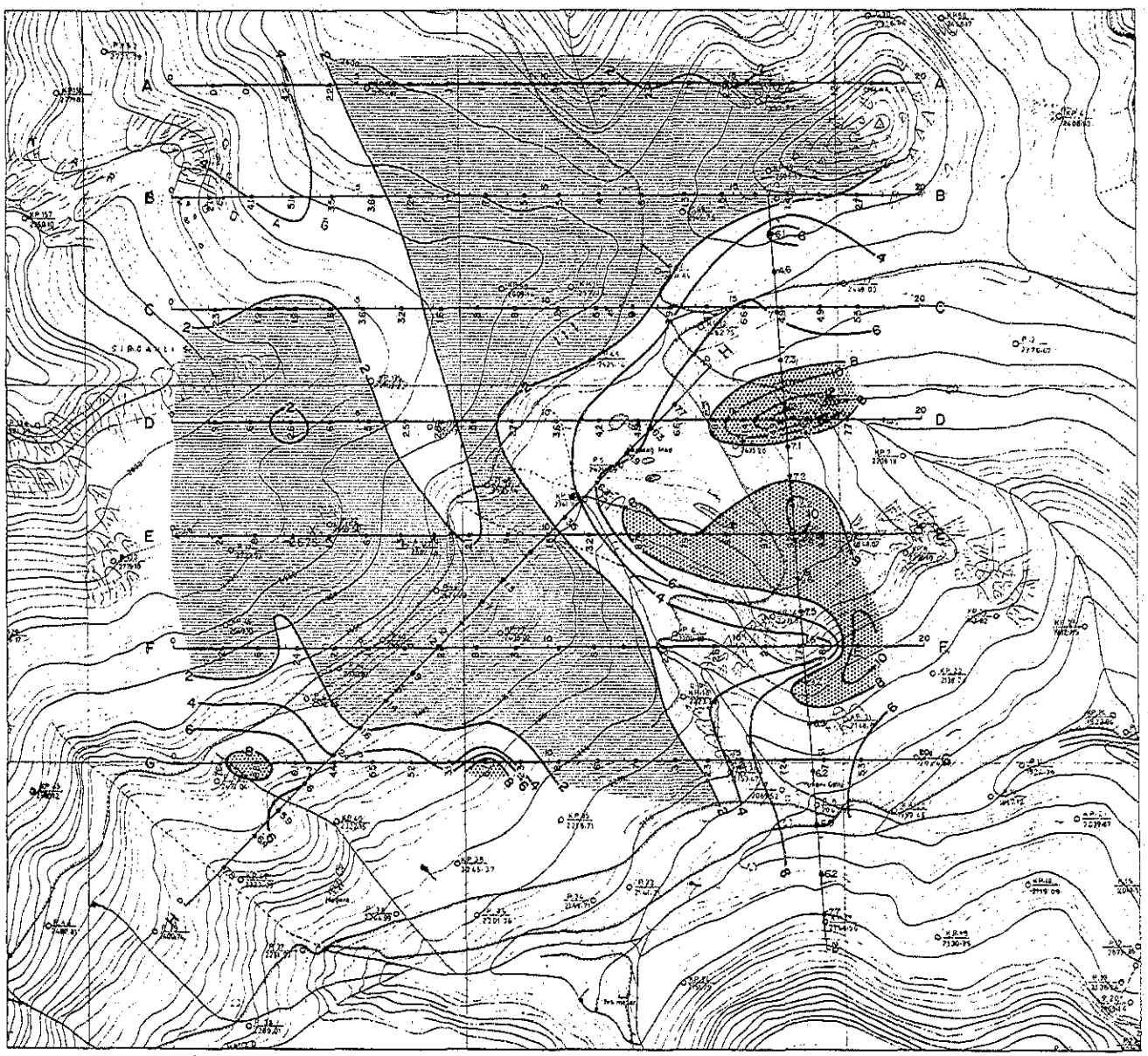

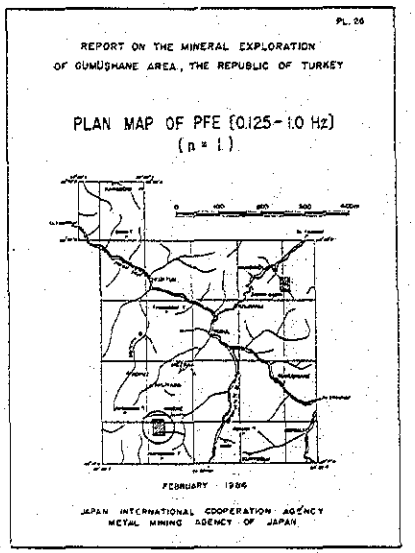

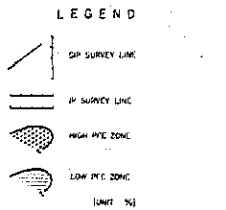

Fig.71 Plan Map of PFE [0.125 - 1.0 Hz] (n = 1)

Plan map of n = 3 (Fig. 72)

A anomalous zone of larger than 8% has the same distribution as the case of n = 1, although it shifts to the north side (namely between Lines D and E) at the eastern part, showing the boundary of andesite lava and quartz andesite. A PFE anomalous zone extends at the western part of Line G, distributed at the border of quartz porphyry and andesite lava.

Plan map of n = 5 (Fig. 73)

Distribution of the PFE values generally follow the same tendencies as n= 1 and n= 3, but it shifts to the west at the eastern part.(namely around Maden Stream). The anomalous zone extends its distribution to the south-western part of the surveyed area. Small anomalous zones, on the other hand, were detected on Line E (central part of the surveyed area) and at the eastern part of Line B.

Pseudo-Section of Percent Frequency Effect

Pseudo-section of PFE (Fig. 74)

Pseudo-sections of PFE are compiled on panel sections like the sections of the apparent resistivity. A distinct pattern of anomalous PFE exists at the shallow part of eastern Line E. At the eastern part of Line L, a PFE anomalous source originates at depth, and expands into a mushroom-form toward the shallower part. A negative PFE anomalous zone is present at the deep part of No.12, and another PFE anomalous zone exists at deoth between No.9 and No.11 on Line L.

On Line F, PFE values increase remarkably at the east end of the line, and tends to extend further toward the outside of the surveyed area. there are high PFE values larger than 11 % in the neighbourhood of negative PFE anomalies around Maden Stream, and they continue south to the anomaly at the east part of Line G. On the other hand, at the west part of Line G, two PFE anomalies forming an up-side-down pant-leg pattern are present- at the lower part between No.2 and No.6, and between No.7 and No.9. They may originate from different sources.

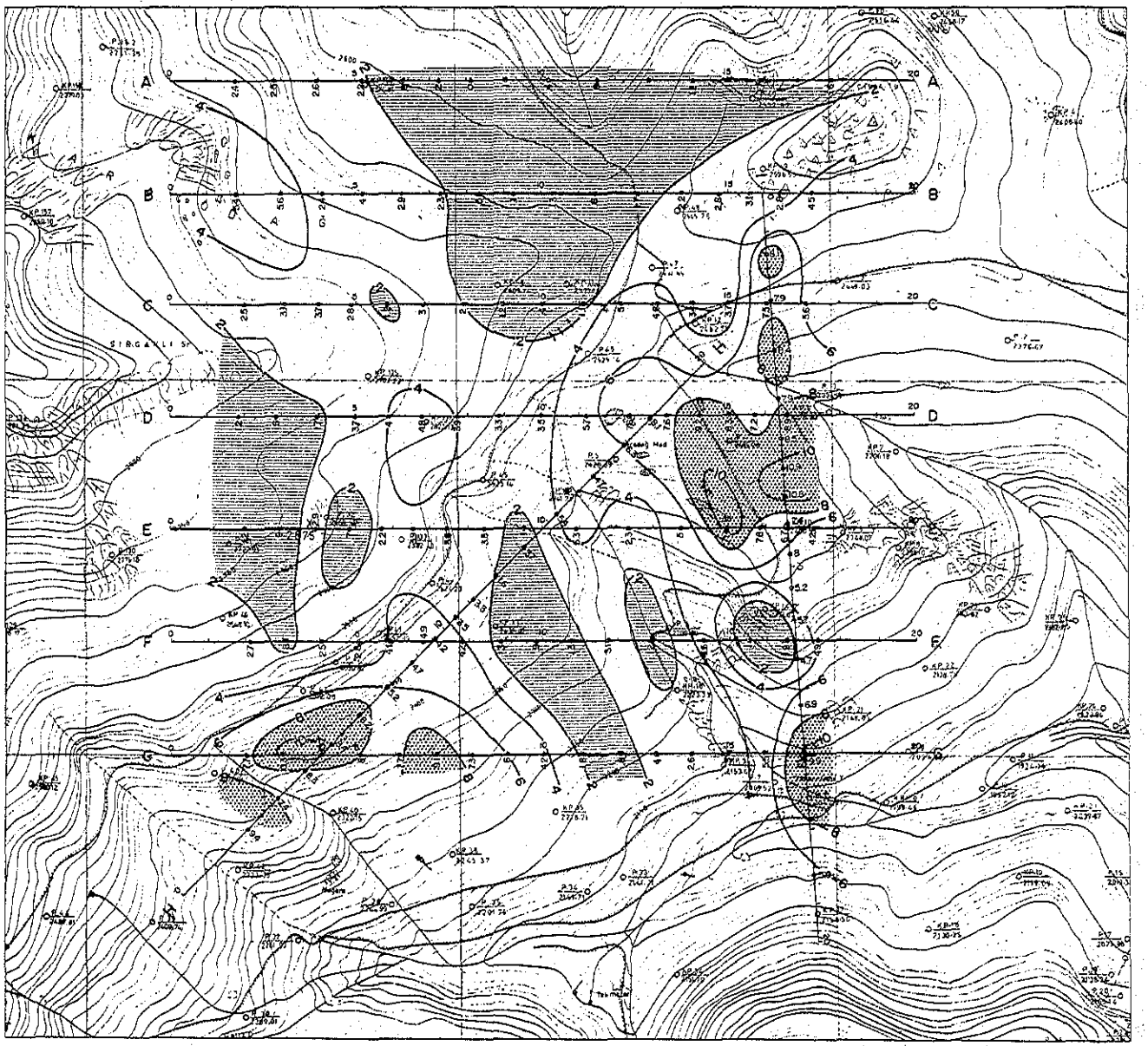

REPORT ON THE MINERAL EXPLORATION
OF GUMUSHANE AREA, THE REPUBLIC OF TURKEY

PLAN MAP OF PFE (0.125 - 1.0 Hz)
(n = 3)

FEBRUARY, 1986

JAPAN INTERNATIONAL COOPERATION AGENCY
METAL MINING AGENCY OF JAPAN

LEGEND

SMP SURVEY LINE

TP SURVEY LINE

HIGH PFE ZONE

LOW PFE ZONE

Fig.72 Plan Map of PFE [0.125 - 1.0 Hz] (n = 3)

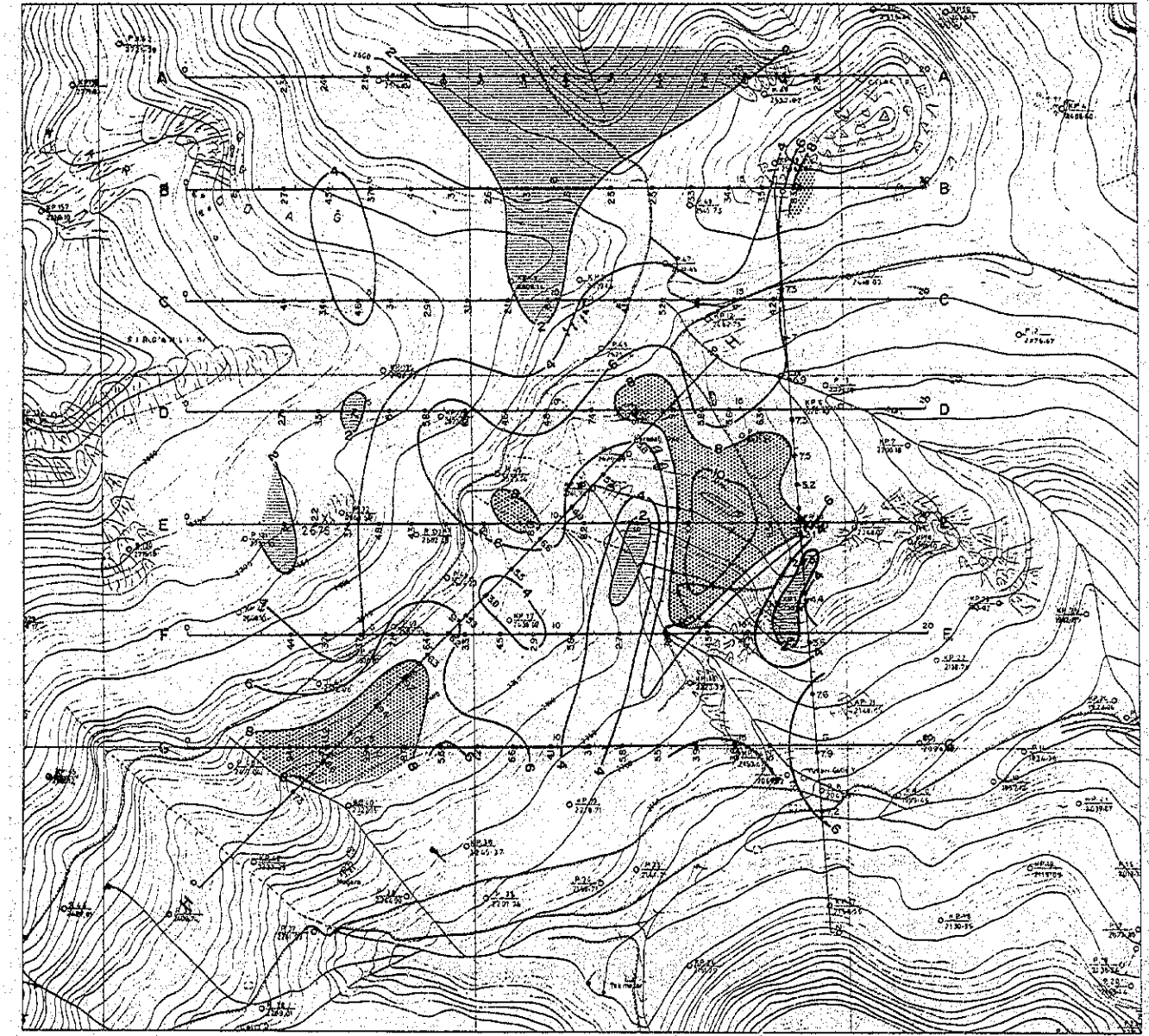

PL. 28

REPORT ON THE MINERAL EXPLORATION
OF GUMUSHANE AREA, THE REPUBLIC OF TURKEY

PLAN MAP OF PFE (0.125 - 1.0 Hz)
(n = 5)

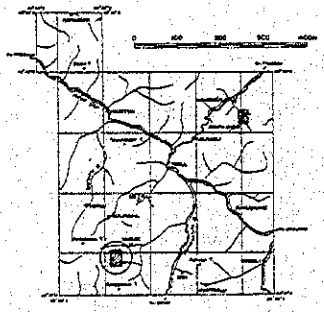

FEBRUARY 1986

JAPAN INTERNATIONAL COOPERATION AGENCY
METAL MINING AGENCY OF JAPAN

LEGEND

SP. SURVEY LINE

IP SURVEY LINE

HIGH PFE ZONE

LOW PFE ZONE

(UNIT : %)

Fig.73 Plan Map of PFE [0.125 - 1.0 Hz] (n = 5)

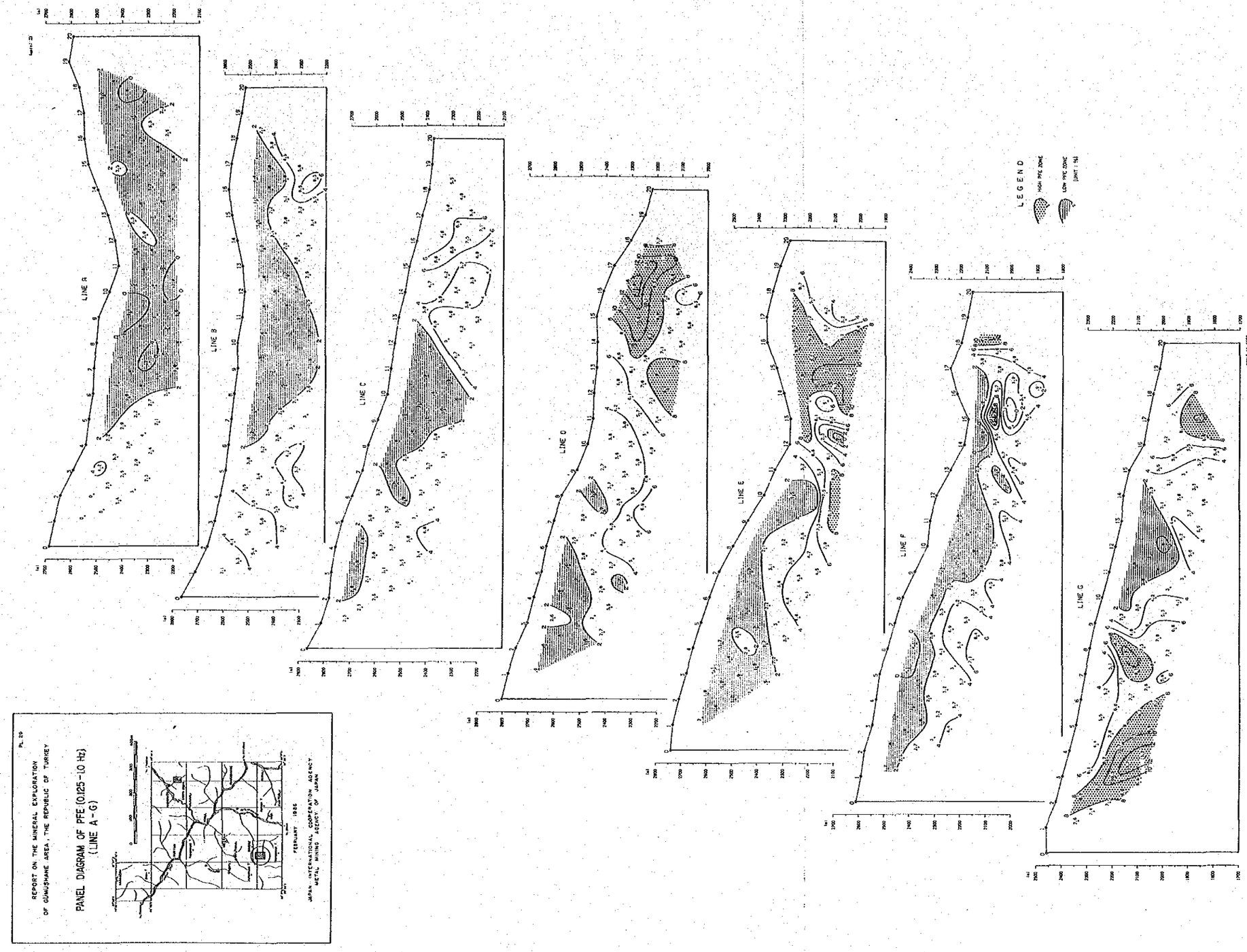

Fig.74 Panel Diagram of PFE (Line A - G)

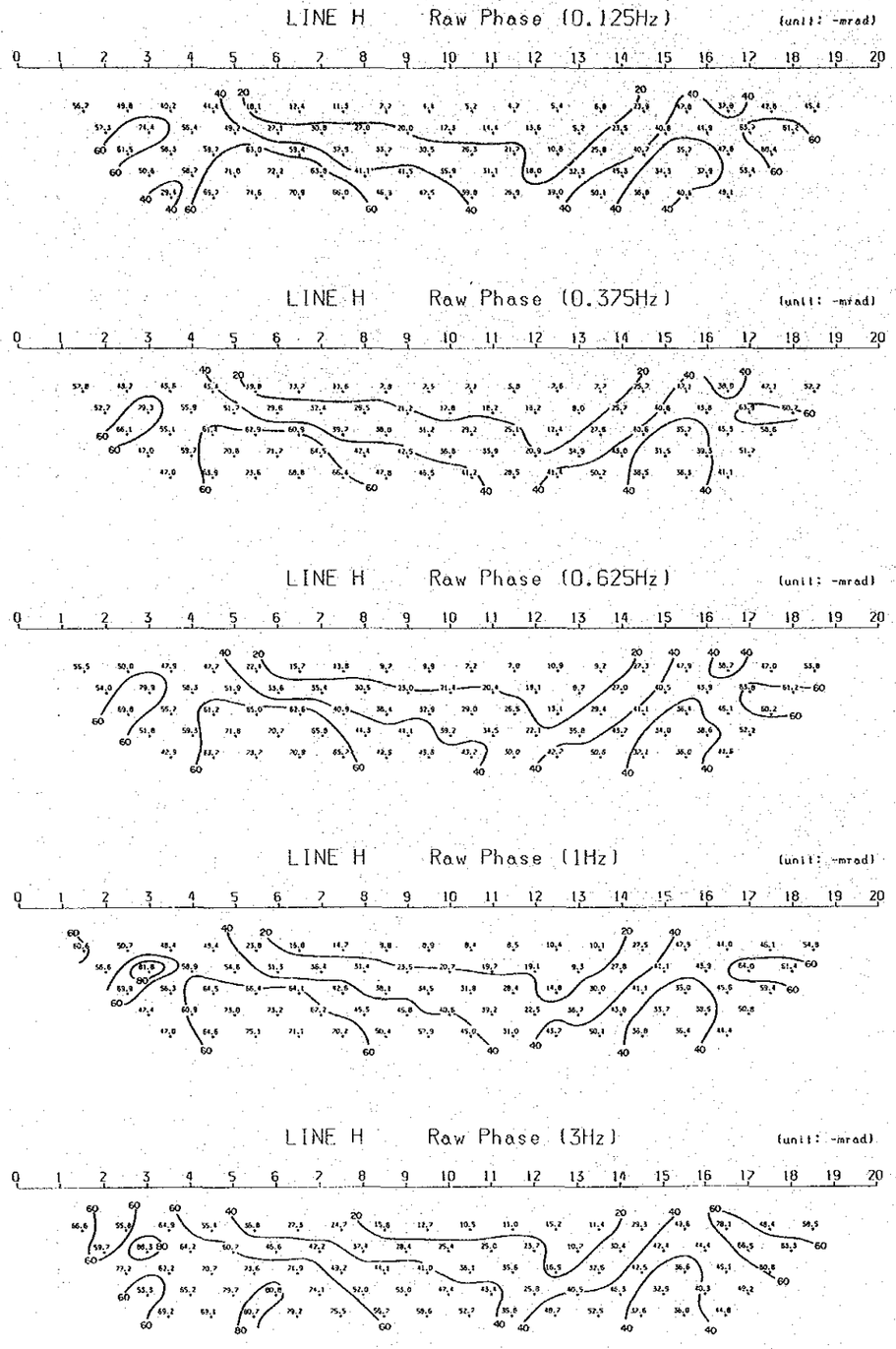

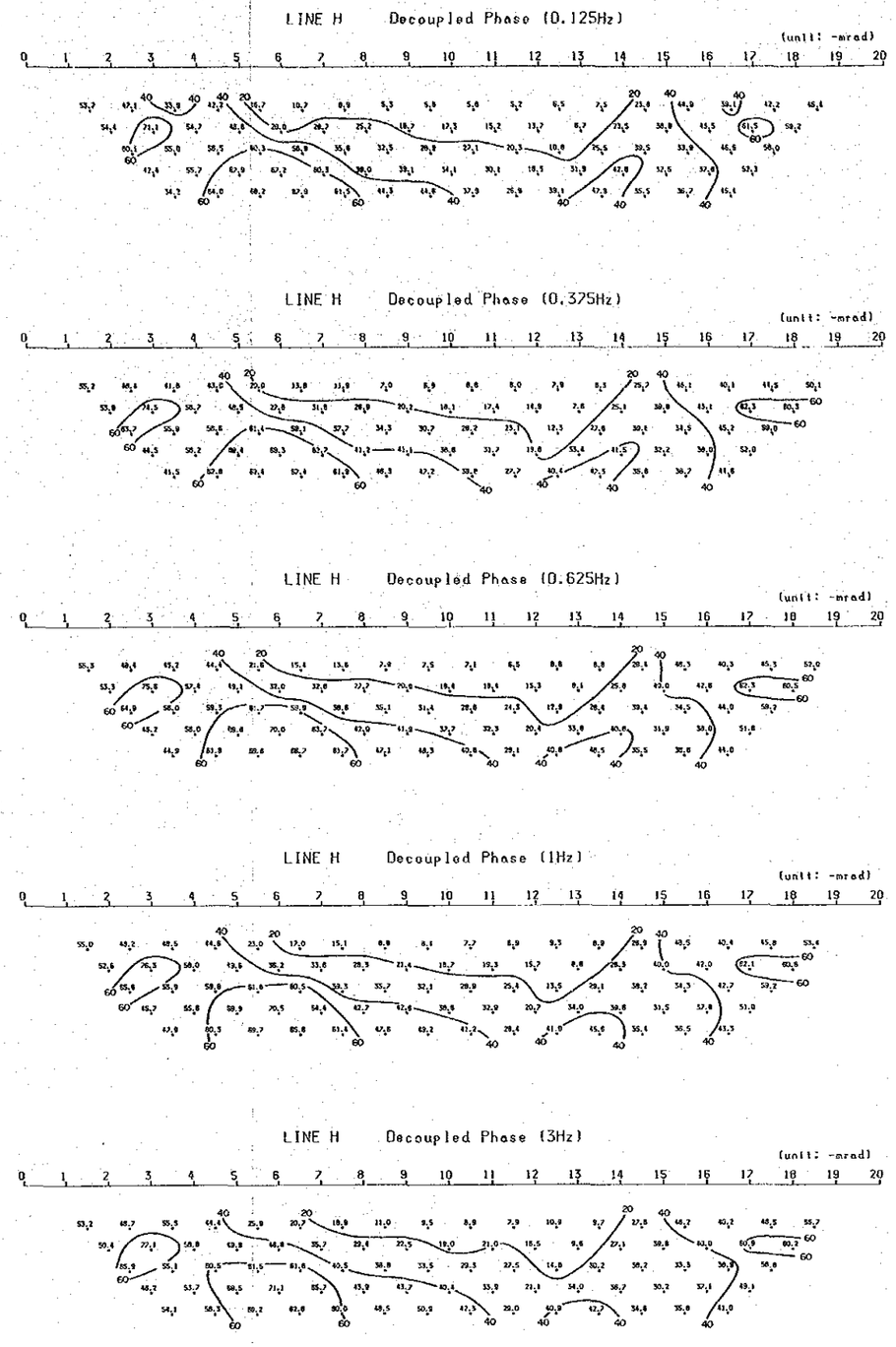

Fig.75 Phase Difference at Five Frequencies (Line H)

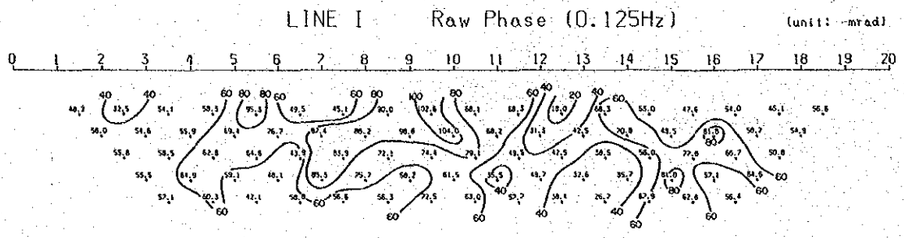

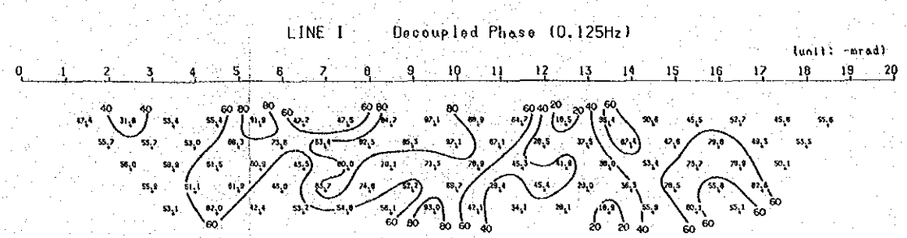

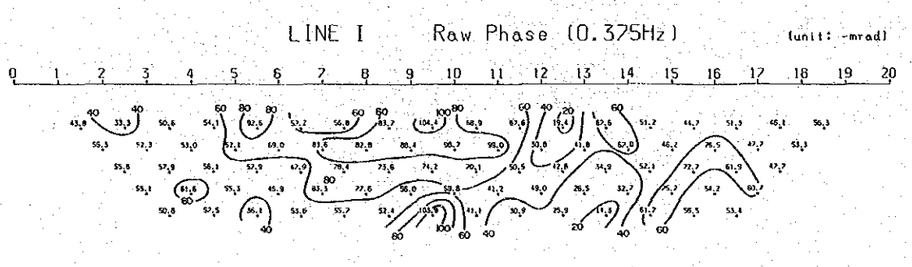

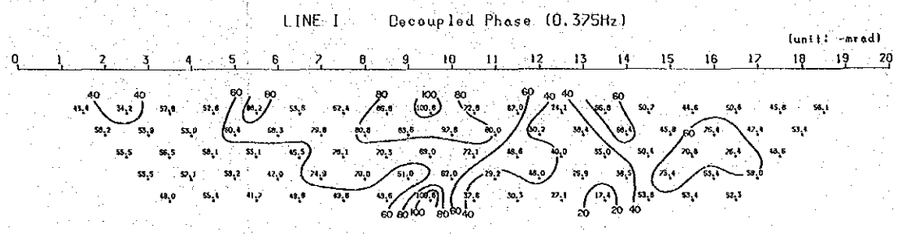

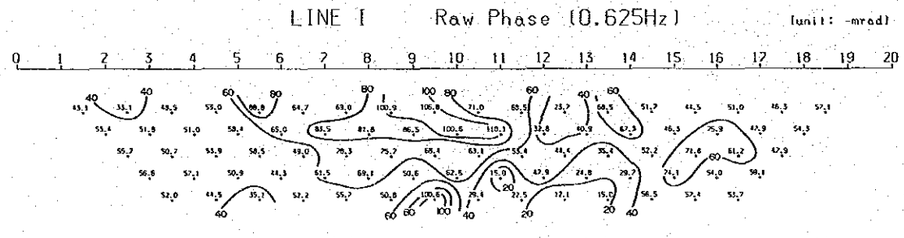

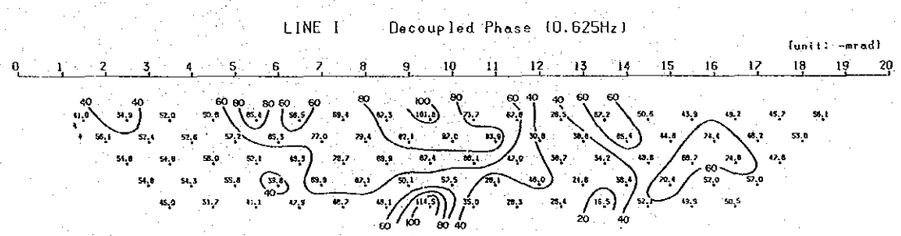

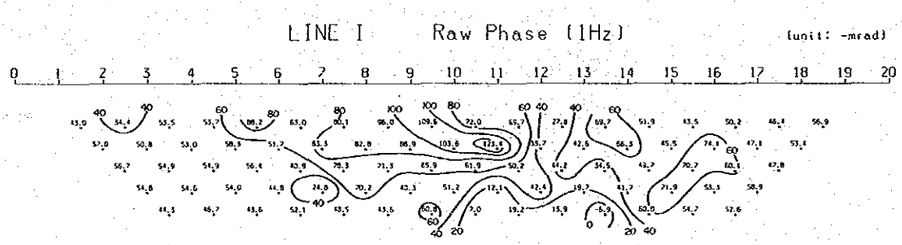

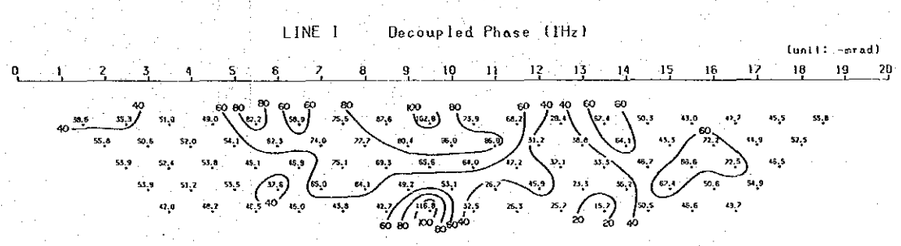

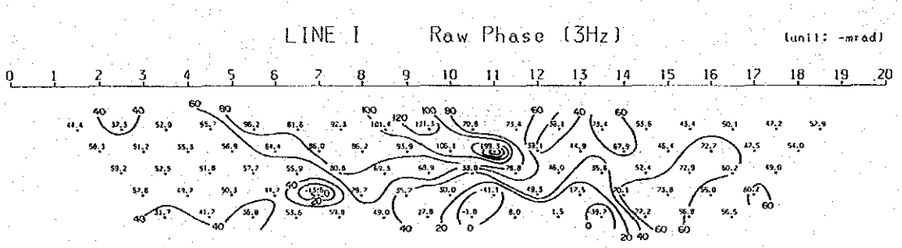

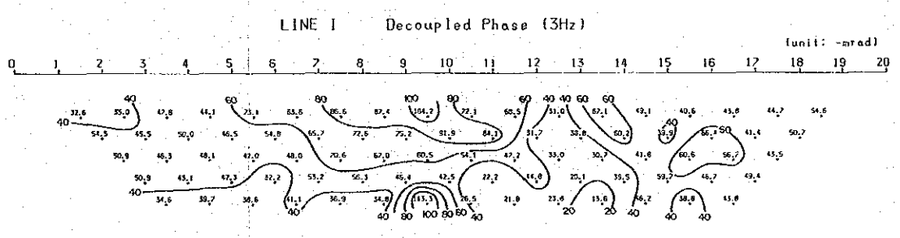

Fig.76 Phase Difference at Five Frequencies (Line I)

Line H (Fig. 69 PFE)

Two PFE anomalies were detected at the south-western part and at the north- east end of Line H. The former consists of an 11.1 % value part and a part between No.4 and No.8, as a pair forming an up-side-down pant-leg pattern. The anomaly was detected at the boundary of andesite lava and quartz porphyry which intruded into the andesite.

On the other hand, the latter may originate from a shallow source, although its shape is undefined.

Line I (Fig. 70 PFE)

Three PFE anomalies were detected at the shallow part of the center of the line, at a part between No. 14 and No.17 along Maden Stream, and at the north end of the survey line. The two former anomalies form the typical pant-leg pattern originating from a shallow anomalous source, and the anomaly at the center part of the line was detected at the boundary between basaltic lava and quartz porphyry. The third is situated at the boundary between diorite and andesite lava located at the end of the line, and may extend more into the northern part.

(3) Pseudo-Sections of Phase

For two lines (H and I), pseudo-sections of phase were drawn with five frequencies of 0.125 Hz, 0.375 Hz, 0.625 Hz 1 Hz and 3 Hz, and influence of the phase by variation of phase was analyzed.

Line H (Fig. 75)

The pseudo-sections of 0.125 Hz, 0.375 Hz, 0.625 Hz and 1 Hz all show the same contour pattern, while an area of 60 mrad expands somewhat in the pseudo-section of 3 Hz. Accordingly, it is presumed that an electromagnetic coupling influence is scarecely present in the phase. Decoupled phases do not vary at all. Therefore, it indicates complete decoupling.

Line I (Fig. 76)

The pseudo-sections of 0.125 Hz,0.375 Hz and 0.625 Hz show the same contour pattern, whereas the zone over 60 mrad in phase value increases on the pseudo-sections of 1 Hz and 3 Hz.

However, decoupled phases show the same pattern for all sections of the five frequencies.

The pseudo-sections of phase of Lines H and I indicate that phases of high frequency are also not variable, since the influence of electromagnetic coupling influence was quite small. Even this small influence was removed completedly by decoupling treatment.

(4) Phase, Magnitude and Cole-Cole Spectra

Pseudo-sections were compiled on phase, magnitude and Cole-Cole spectra , and these decoupled spectra were also drawn together. The spectra on each pseudo section are explained as follows :

Line H (Fig. 77)

(A) Phase spectrum

Phase spectra are roughly grouped into two types. Namely, one type is flat at the part from 0.125 Hz to 1 Hz, and increases from 1 Hz. The other type increases simply from 0.125 Hz. This is caused by small phase values in an area of low frequency. The former is present at the south-western part and north-eastern part of the line, and the latter is observed in shallow parts at the center of the line. The difference between both types depends on large or small values of phase at 0.125 Hz and on PFE. That is, the former spectrum occurs in the strongly mineralized part, while the latter phase is mainly present in the unmineralized zone.

Decoupled phase spectra are definitely divided into flat type and simply increasing type. Some flat type forms convex upward at the part between No.5 to No.7.

(B) Magnitude Spectrum

Magnitude spectra which are steeply decending to the right are observed at both ends and in deep parts of the line. The spectrum is nearly flat at the center of the line. Decoupled spectra are also similar in their form.

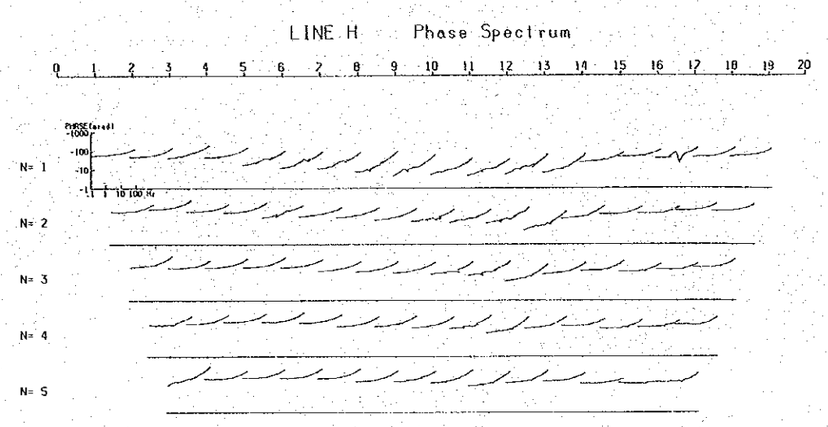

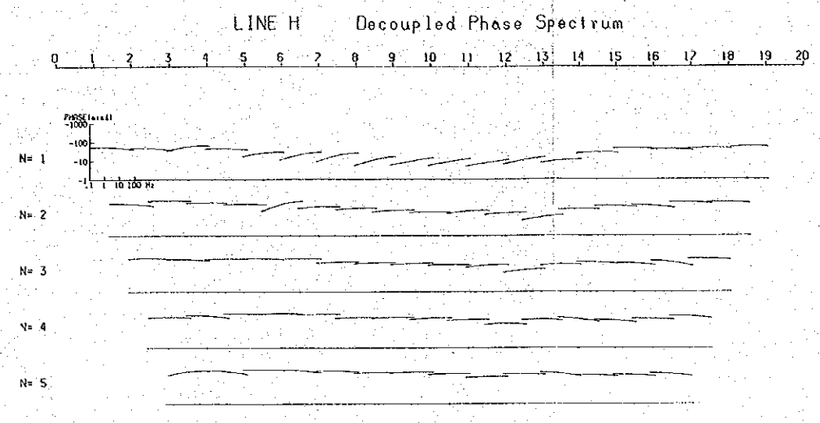

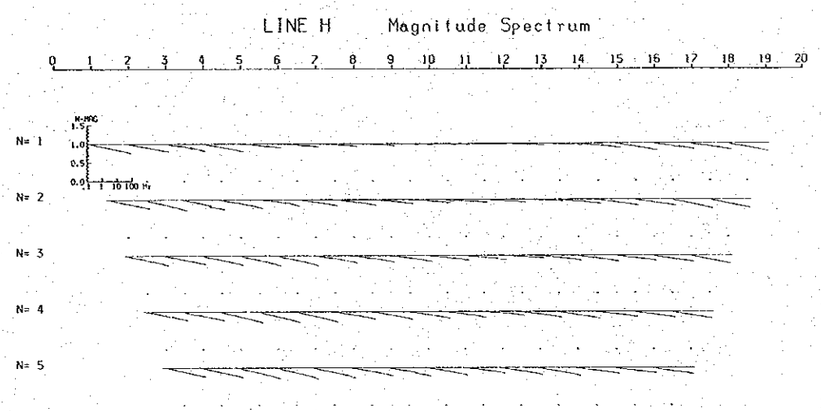

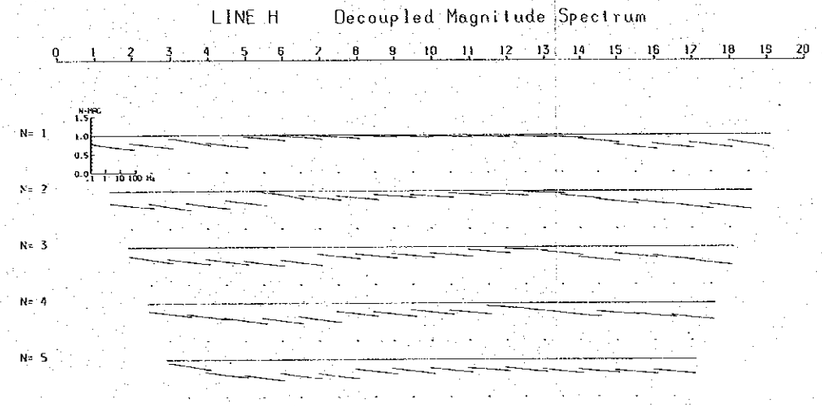

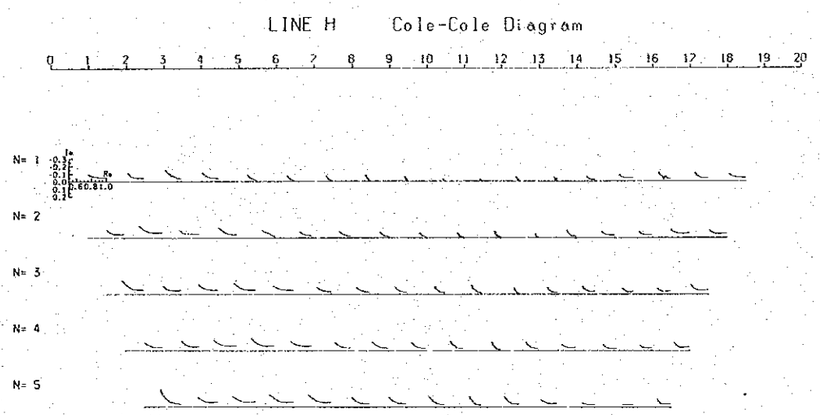

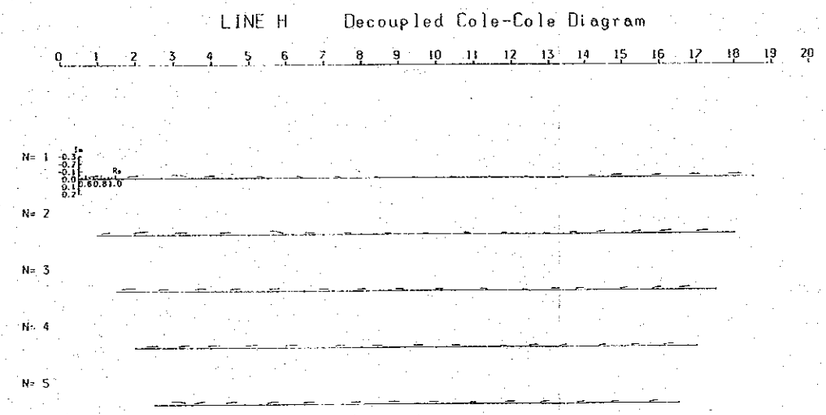

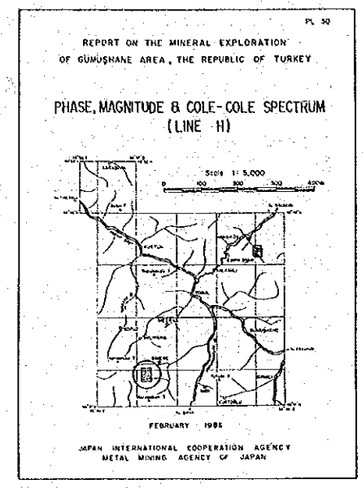

Fig.77 Phase, Magnitude and Cole-Cole Spectrum (Line H)

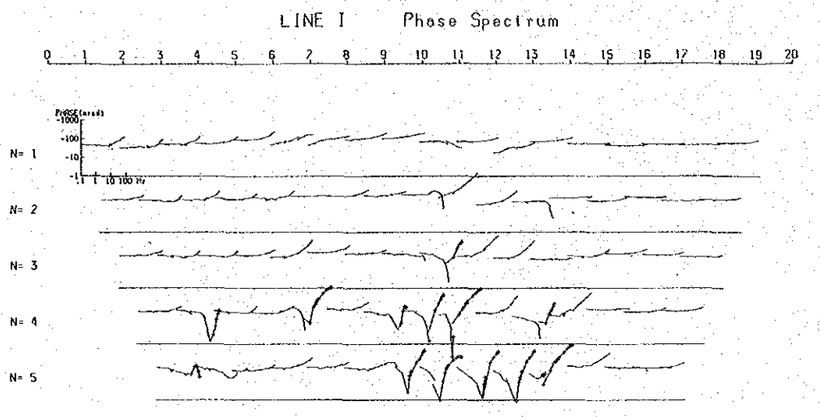

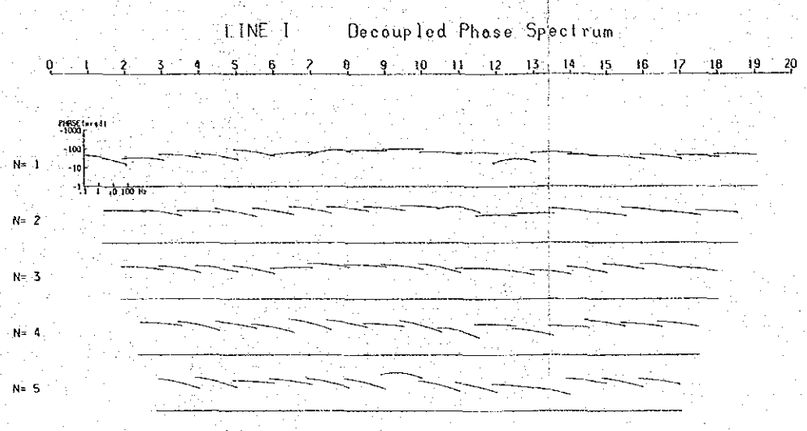

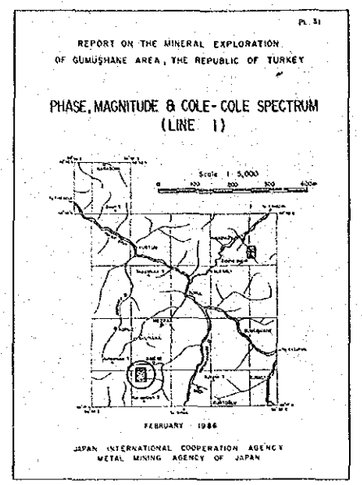

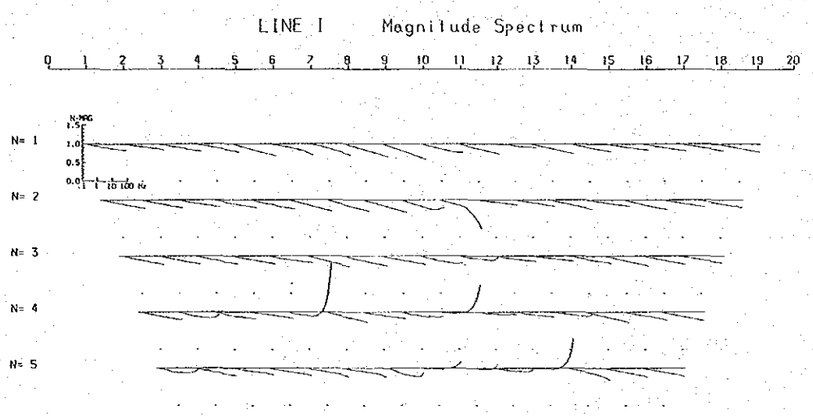

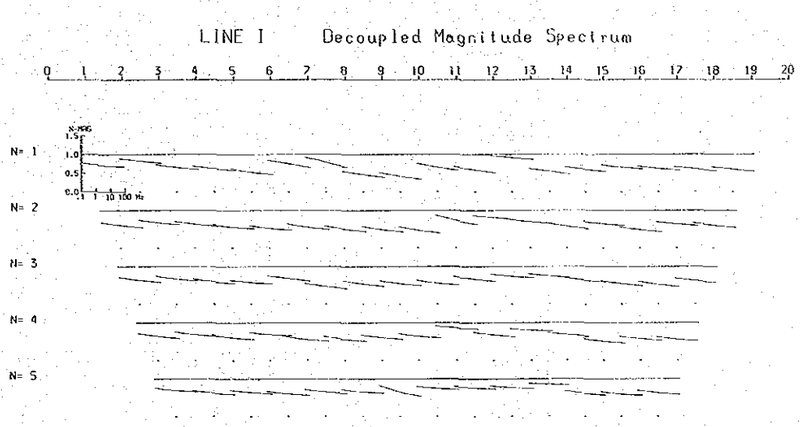

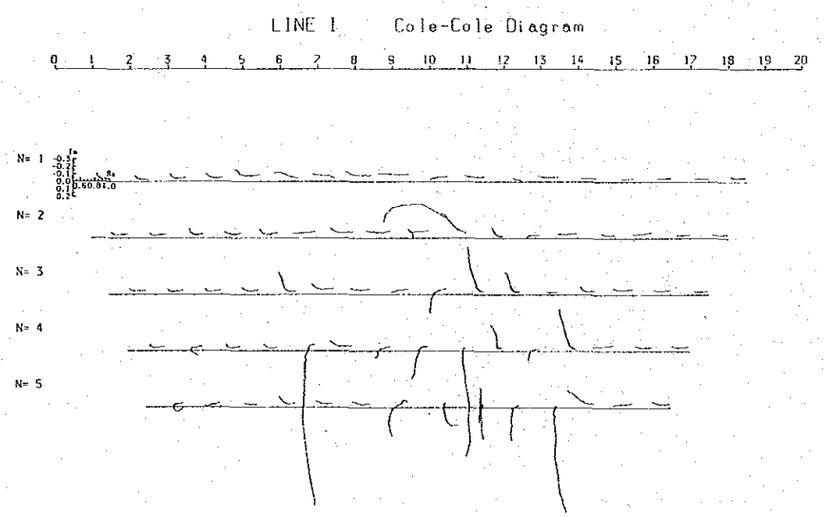

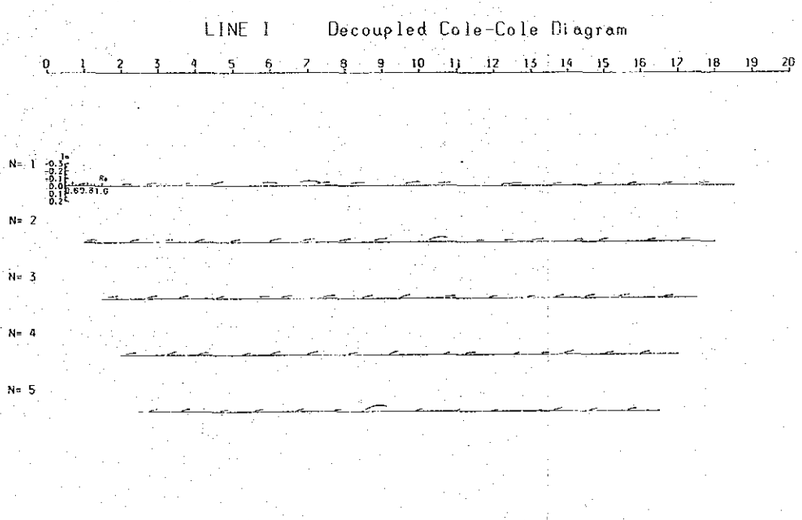

Fig.78 Phase, Magnitude and Cole-Cole Spectrum (Line I)

(c) Cole-Cole diagram

Most Cole-Cole diagrams show descent to the right. A length of arc on the linear part of the diagram is longer at both ends of the survey line, whereas it is shorter at the center of the line. After the decoupling process, two diagrams of flat spectra are observed. The flat diagram type corresponds to the part with the large values of phase and PFE.

Line I (Fig. 78)

(A) Phase spectrum

Phase spectra were detected as two types; namely, one is nearly flat, and the other occurs as negative noise at deep sections of the center line. The spectra generally observed more noise and disturbance in contrast with spectra of the other survey lines. This was caused by small input voltage, large earthing resistance resulting in difficult currency, and low resistance underground. The negative phase occurs at the contact between low apparent resistivities of less than 10 ohm-m and high apparent resistivity. This phenomenon is usually called pipe-line effect.

Decoupled phase spectra consist of two types: flat (or convex upward) and descending to the right. The former type was detected at shallow depths from No.6 to No.11 on the line, corresponding to the PFE anomaly zone.

(B) Magnitude spectrum

Characteristic spectra which dip steeply and descend to the right are observed at the center part of the line. Three spectra which suddenly ascend steeply at high frequency were detected, corresponding with the part of anomalous negative phase spectrum.

(C) Cole-Cole diagram

Five spectrum types are recognizd- flat B-type, descent-to-right C-type, ascent-to-right A-type, and two peculiar types of ascension and descension. The A-type is common in the south half of the line and C-type is common in the north half of the line. Decoupled spectrum diagrams are mostly ascent-to-right types and with some flat type parts. Among the diagrams, a spectrum diagram presumed to relate to mineralization is located at shallow depths from No.5 to No.9.

(5) Decoupled Percent Frequency Effect

Decoupled phase spectrum, magnitude spectrum, and Cole-Cole diagram of five frequencies are described above. In the article, it is mentioned how PFE values were varied after the decoupling process.

Line H (Fig. 79 upper figure)

The PFE values are scarecely influenced by electromagnetic coupling, resulting in similar spectrum patterns before and after the decoupling process.

Line I (Fig. 79 lower figure)

The decoupled PFE values are generally unvaried from pre-decoupled values, but the 14 % of the PFE value occurs as a larger value than that in pre-decoupled at No.9 to No.10. In this area, low apparent resistivity values less than 10 ohm-m are also present, showing the existance of some mineralization.

(6) Model Simulation for IP anomaly

Line D (Fig. 80)

A model simulation was processed for the PFE anomaly in the area of basaltic lava distributed at the eastern part of the line. A high resistivity basaltic lava (code 3) accompanied by mineralization is simulated in the shallow part, while a somewhat low resistivity, high PFE-anomalous source (code 6) is presumed to exist at depth.

The result indicates that the simulated pattern is similar to the observed pattern. The anomalous source is inferred to continue from the shallow part of No.16 to the deeper part with a dyke form, suggesting the existence of strong partly mineralized quartz porphyry .

Line G (Fig. 81)

A model simulation was processed on the up-side-pant-leg pattern in the western part of the line. Quartz porphyry (code 1) and andesitic lava (code 2 and code 3) are extensively distributed

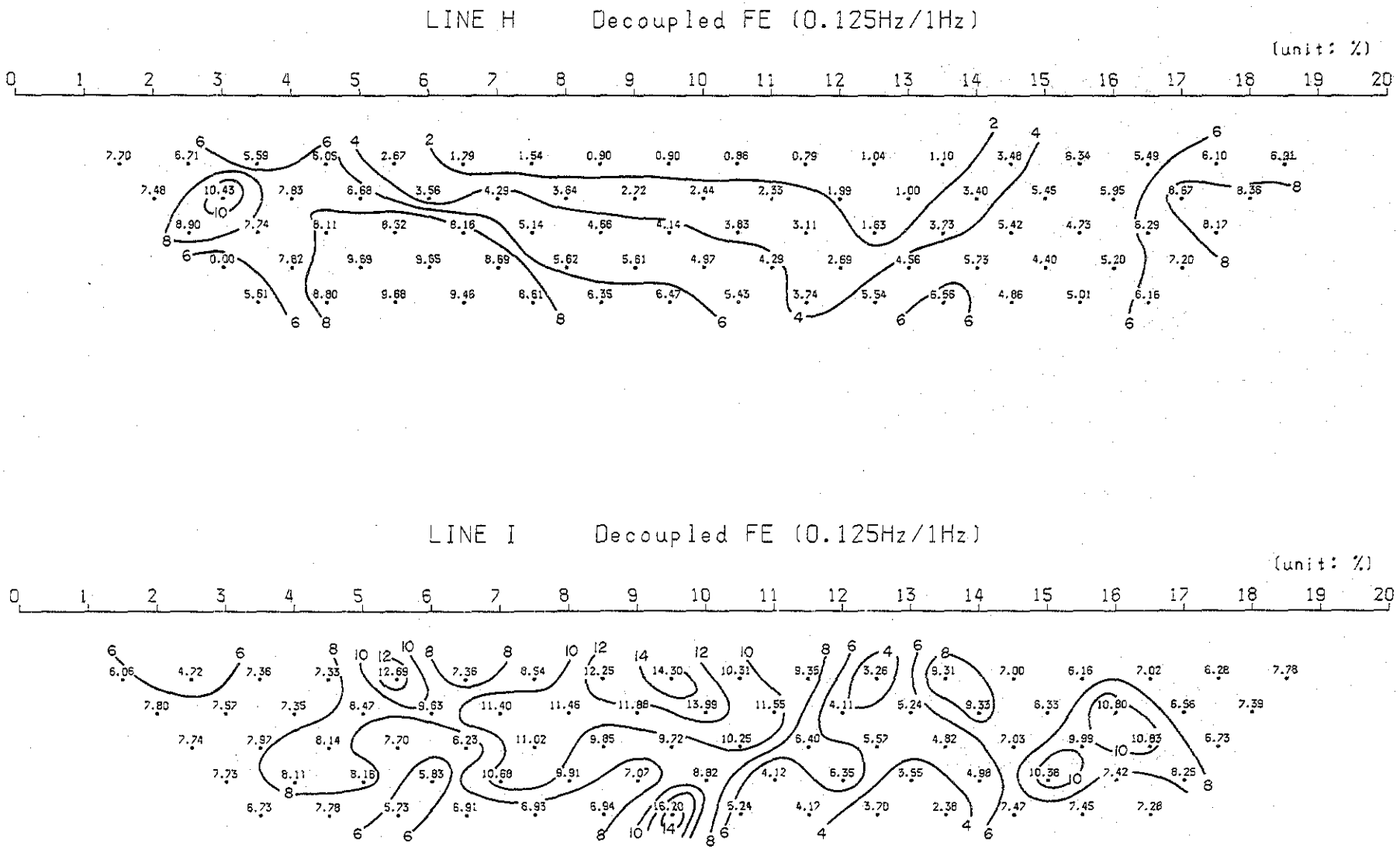

Fig.79 Decoupled PFE (Line H, Line I)

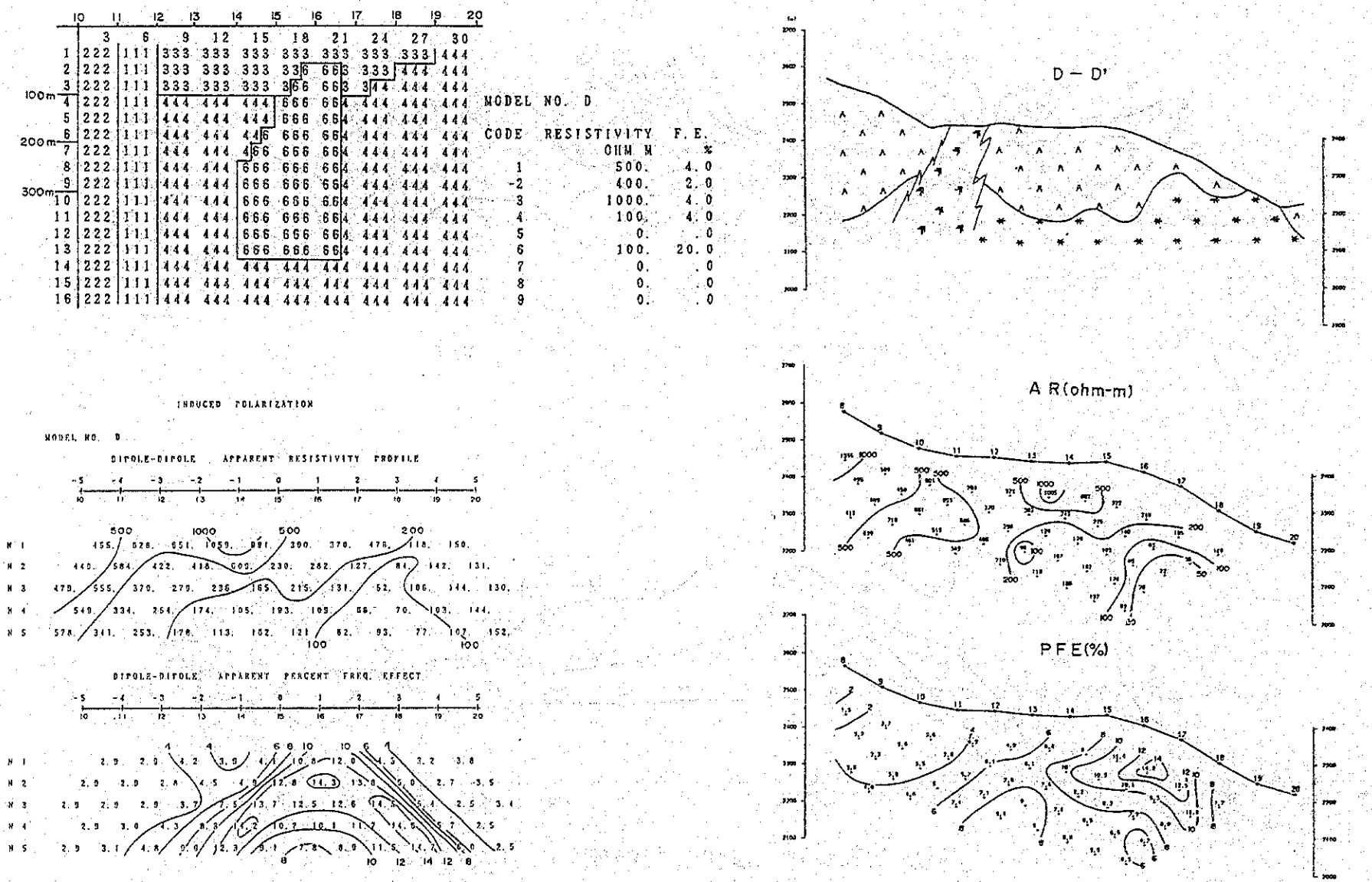

Fig.80 Result of Model Simulation (Line D)

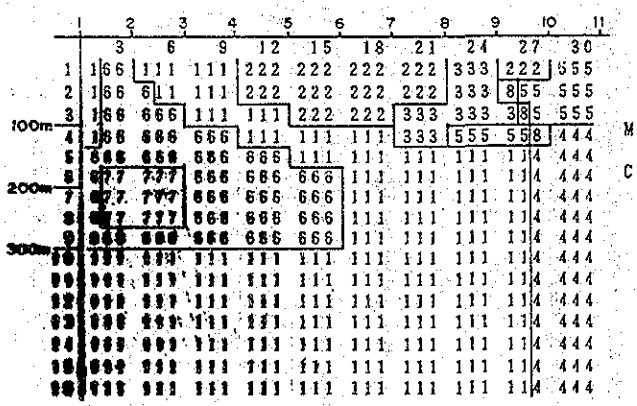

MODEL NO. G

CODE	RESISTIVITY OHM M	F.E. %
1	400.	6.0
2	500.	4.0
3	1500.	4.0
4	100.	4.0
5	100.	1.0
6	400	10.0
7	100.	50.0
8	100.	30.0
9	0.	.0

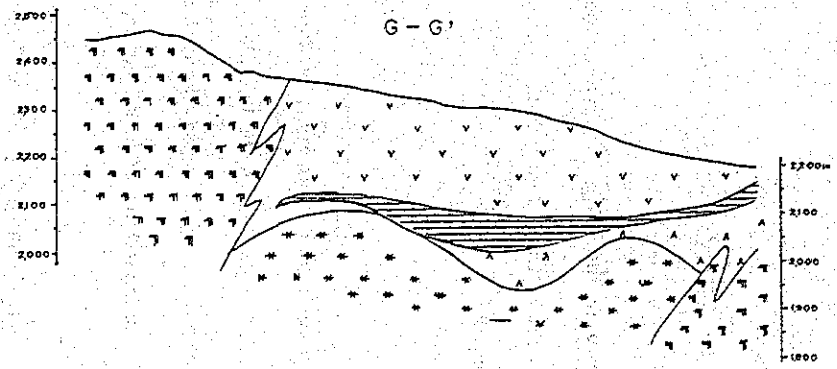

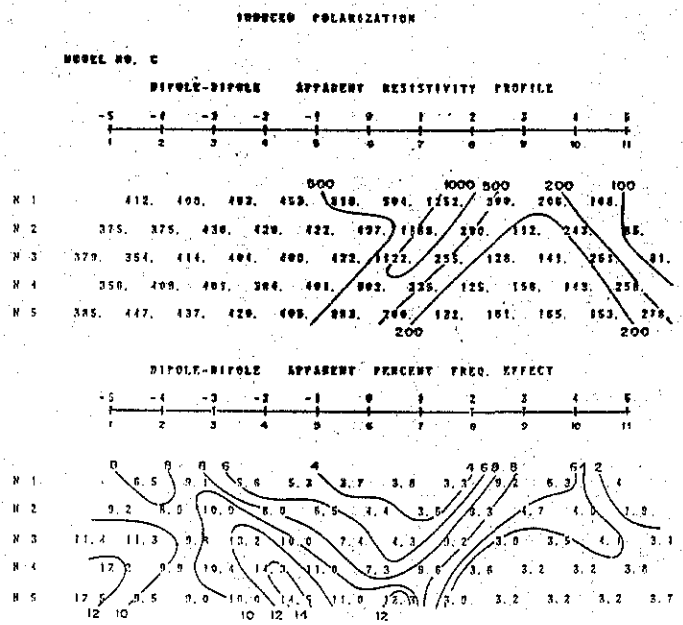

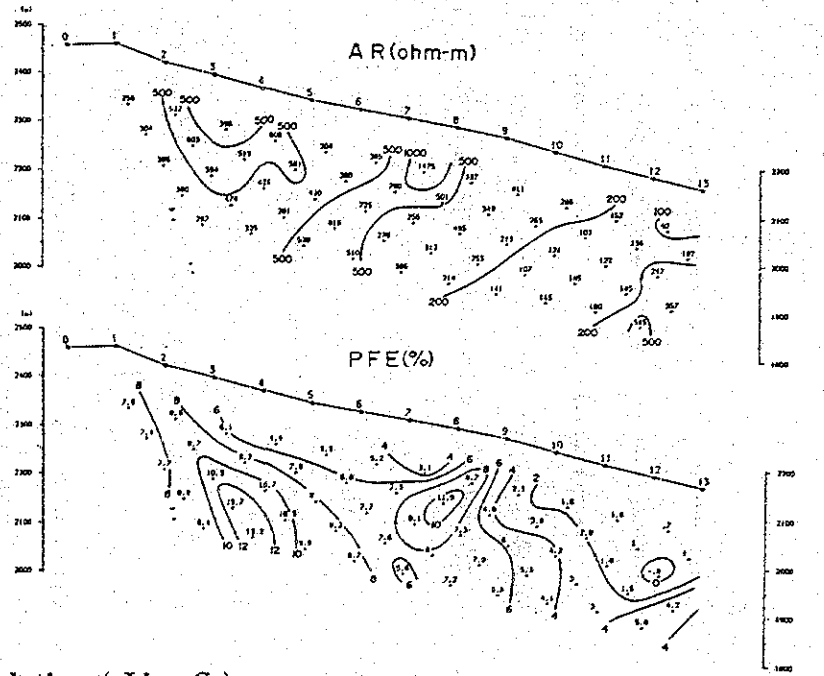

Fig.81 Result of Model Simulation (Line G)

at the western part of the survey line, and anomalous sources named codes 6,7 and 8, are simulated at the boundary between both rocks.

The simulated patterns fit well with observed ones, proving that their simulated model is appropriate. The anomalous source is large in scale and massive in form, and it might be caused by mineralization associated with the the quartz porphyry intrusion.

Line I (Fig. 82)

This survey line was laid in a north-south direction to unravel a zone of anomaly continuously detected at the eastern part of Lines D to G. The anomalous part is present at the boundary zone between the basalt (code 2) around No.5 and the quartz porphyry (code 1 and code 5) located at the southern part near No.8. The anomalous source is simulated as code 8, having 100 ohm-m of resistivity and 20 % of PFE.

The simulated pattern is similar to the observed pattern, but the simulated 8 % zone of PFE is distributed in a somewhat more extensive and deeper area, in comparison with the observed zone.

(7) Discussion and Interpretation Map

Discussion

In the survey area, IP and SIP methods of geophysical survey were conducted in the promising mineralized area where skarn and disseminated ore deposits were expected. The survey results are disscussed as follows :

(a) The low resistivity zone was detected on Lines A and B, passing through the area in which the old mine is located, in the northern survey area. The low resistivity zone may be due to underground water coming from melted snow and not from a mineralized alteration zone, since it is situated at an area from mountain ridge to mountain side, where water is flowing from the north side of Line A. PFE values in the low resistivity zone are lower than 1.5 % background value.

(b) The limestone is exposed at the central northern part of the surveyed area, and many old adits which had been used to mine skarn type ores are distributed in the center part of lines B,C, and

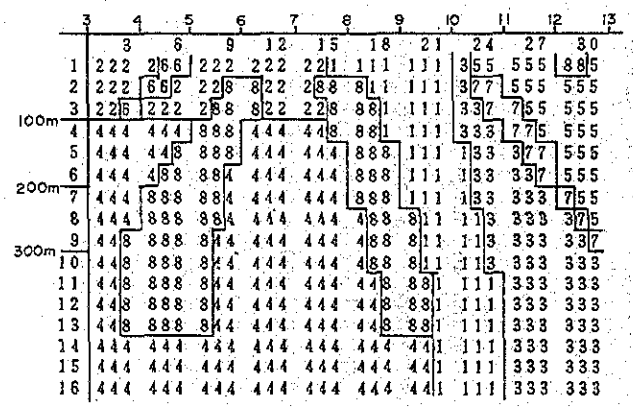

MODEL NO. 1

CODE	RESISTIVITY OHM M	F.E. %
1	300.	6.0
2	400.	6.0
3	400.	4.0
4	100.	4.0
5	500.	4.0
6	1.	8.0
7	1.	4.0
8	100.	20.0
9	0.	.0

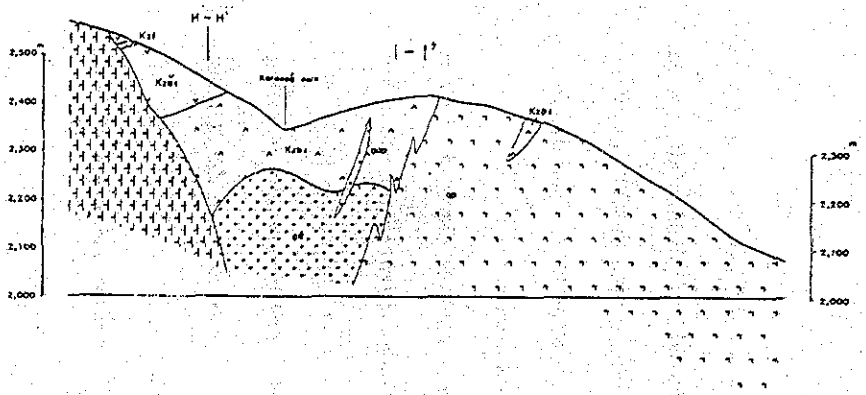

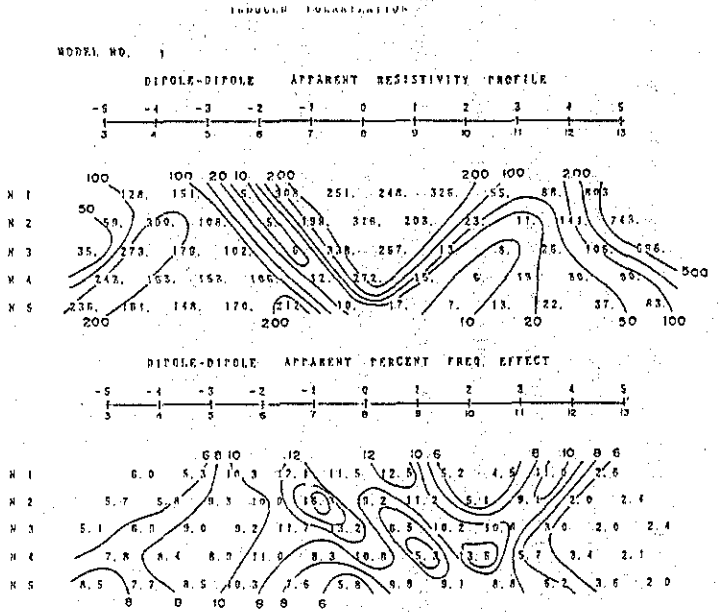

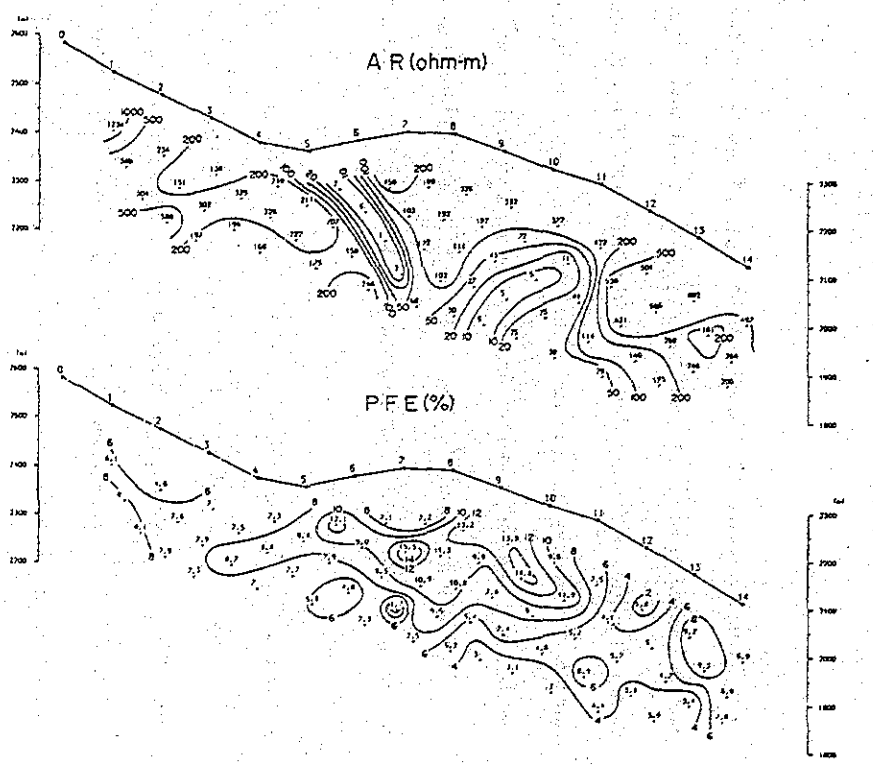

Fig.82 Result of Model Simulation (Line I)

D. However no data indicating emplacement of ore deposit are obtained through the geophysical survey, owing to PFE values of below 1.5 % in that part. It is presumed that the mineralized area is not profitable either by the reason that the ore deposit is smaller in size than the 300 m of the survey line spacing and the 100 m of the station intervals in the geophysical survey specifications or that it is embedded at only shallow depths part and the ores are oxidized.

On the other hand, another PFE anomaly was obtained at the center and at depth on Line E on the west side of the limestone dipping 45° and distributed along Maden Stream from the center and south east part of the survey area. This anomaly is supposed to be caused by skarn type mineralization since the limestone would be distributed at the location of the PFE anomaly, according to the noting from geological information, in spite of the different mode compared with the anomaly caused by dissemination type mineralization observed at the east part.

The low reistivity zone with high PFE values in the center part of survey lines E and F along Maden Stream is also a promising area, judging by the geological imformation.

(c) The dissemination type PFE anomaly zone was obtained at the eastern and south western part of the survey area. The former is located in basaltic lava and the latter is distributed at the boundary between andesite lava and quartz porphyry. A mineralization accompanying the quartz porphyry intrusion is expected in the area, although mineralized showings are not observed.

(d) Twenty five rock samples were measured to determine SIP property. The result indicates that values of phase and PFE are larger in mudstone, while smaller in limestone and andesite lava. The values of resistivity are mostly high, with only two samples below 500 ohm-m.

On the phase spectrum, ten samples belong to the A-type diagram, and three samples are categorized into the X-type diagram and are related with mineralization. Among the X-type samples, the two black mudstone samples have large values of PFE and phase, while one sample of quartz porphyry has samll values of phase and PFE. On the other hand, a mudstone sample having a 10.4 % value of PFE is grouped into the B-type spectrum.

That result reveals that special relationship between phase and PFE values are not recognized.

Interpretation Map (Fig.83)

PL. 32

REPORT ON THE MINERAL EXPLORATION
OF GÜMÜŞHANE AREA, THE REPUBLIC OF TURKEY

GEOPHYSICAL INTERPRETATION MAP OF THE KARADAĞ AREA

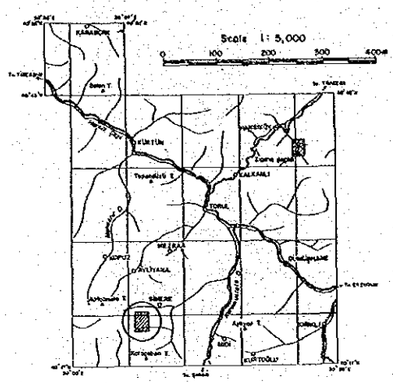

FEBRUARY · 1986

JAPAN INTERNATIONAL COOPERATION AGENCY
METAL MINING AGENCY OF JAPAN

LEGEND

- SIP SURVEY LINE
- IP SURVEY LINE
- HIGH PFE ZONE (6 %)
- LOW PFE ZONE (2 %)
- HIGH RESISTIVITY ZONE (500 ohm-m)
- LOW RESISTIVITY ZONE (50 ohm-m)

Fig.83 Geophysical Interpretation Map in the Karadağ Area

The result of the geophysical survey is summarized and point out the following :

① The anomaly distributed at the stream at the east end of Line D in the east survey area originats from an anomalous source (strongly mineralized zone) embedded at shallow depths. It is presumed to be an anomaly caused by sulphide ore (pyrite).

② The anomaly of the south west survey area results from a deep anomalous source, and is inferred to be related with quartz porphyry. Another anomaly in the south area is embedded in quartz porphyry down from Maden Stream, and is from a shallow anomalous source.

③ The PFE anomaly of greater than 8 % in value was detected at depth on the western side of Maden Stream (Line E) corresponding to the limestone strata on the geological profile. The result presumes that the anomaly is a skarn type ore deposit.

④ The limestone in the north survey area is regarded as the old Karadag mining area owing to the scattering of many ore boulders on the surface. However, the PFE responses in the area are less than 8 % in value. The result indicates that the Karadag ore deposit may be embedded only at shallow depths, that it might have undergone oxidation, or that it may be a small scale skarn type ore deposit.

The interpreted result is summarized in Fig. 83. The following anomalous zones are compiled in the figure :

Low resistivity zone (less than 50 ohm-m) on plan map of apparent resistivity (n= 3).

High resistivity zone (greater than 500 ohm-m) on plan map of apparent resistivity (n=3).

High PFE zone (greater than 8 %) on plan map of PFE (n=3).

Low PFE zone (less than 2 %) on plan map of PFE (n=3).

2-4-4 Relationship between Geophysical Survey and Geological Survey

In the area, mineralization was found in the zone of limestone-siltstone to basaltic andesite strata, striking north-south and dipping west according to the geological survey. The IP method of the geophysical survey was conducted on the seven survey lines 2 km in length with each line 300 m apart (total surveyed length : 14 km) in east-west direction, taking into consideration the mineralization condition. As a result, three high PFE anomalous zones were found at the east, south-west and south-east parts of the survey area. The SIP survey was successively conducted to survey these anomalous areas in detail on the two survey lines of H (NE ~ SW) and I (N ~ S) totaling 4 km in length.

The survey results reveal the following :

① The three anomalies in the east, south-west and south-east parts of the survey area are expected to be disseminated type ore deposits.

② The anomaly at the center part of the survey area is expected to be a skarn type mineralized zone embedded in the limestone stratum.

③ In the skarn zone emplaced in the limestone stratum in the north part ofthe survey area, a PFE anomaly has not been found. The presumed reasons are (a) the ore deposit can not be detected through the specifications applied by the IP and the SIP surveys owing to its small scale or (b)low PFE values are due to shallow emplacement and oxidization of the ore deposit.

Part 3 CONCLUSIONS AND RECOMMENDATION

Part 3 CONCLUSIONS AND RECOMMENDATION

Many ore deposits and mineral showings are known in the survey area. A small amount of mines were operated in the past, but most of them have not been explored. These ore deposits and mineral showings are classified into skarn, vein, and dissemination types. Many outcrops of skarn type ore deposit are known through previous surveys, and only some ore deposits were explored or exploited on small scale in long ago. Several small vein type ore deposits containing high grade ores are also under exploration and operation on a small scale.

Dissemination type ore deposits were not noticeable untill recent because of low grade in ore content. Survey and exploration works have targeted to high grade strata-bound or massive ore deposits (Kuroko ore deposit), and discovered many small scale but high grade ore deposits.

Recently, Sar Cheshmeh Mine (ore researve : 450 million tons, Cu 1.13 % and Mo 0.03 %) of Iran, located at the south east part of the Pontid Belt, and Madet Mine (ore researve : 200 million tons Cu 0.40 %) of Bulgaria also located north west part of the Belt were discovered, exploited and are producing. The possibility of such ore deposits in the Turkish Pontid Belt is of special interest to those involved in mining. In fact, disseminated mineral showings have recently been reported .

In the area, the stock body, intruded the during period from late Cretaceous to Eocene, s accompanied by such mineralization. The mineralization is structurally controlled by the shape of the stock and also by conditions of the marginal part of the stock. High grade ores tend to be emplaced area where fractures and faults are well-formed.

Two types of disseminated ore deposit are expected in the Gümüşhane Area. One is a copper-molybdenum bearing ore deposit and the other is a deposit containing copper, zinc, lead without molybdenum. The former ore deposit is distributed in the Hasandere Area and the latter ore deposit is present with skarn type in the Karadağ Area.

1 Conclusion of the Hasandere Area

Led by the discovery of a copper and molybdenum anomalous area through the stream sediment

geochemical survey conducted by the United Nations Development Program during the period from 1970 to 1974 in the Hasandere Area, geological and stream sediment geochemical surveys of the cooperative exploration survey was commenced in 1984. MTA also carried out additional soil geochemical survey. The soil geochemical survey resulted in the detection of values five to nine times higher than values in stream sediments. It was presumed that the Cu and Mo anomalous area had a range of 1.7 km X 1.4 km, and might extend toward the northern and north-western side. Through additional soil geochemical survey in the initial phase the presumption was proven to be correct. The anomalous area extended 1.8 km X 1.8 km as predicted.

Alteration, detected by X-ray diffraction analysis and microscopic observation, is zoned from the center of the altered porphyritic granite (Pgl) toward the marginal part as potassic zone → phyllic zone → propylitic zone. The core of Pgl is a potassic zone of alteration and the alteration changes to a phyllic zone in the periphery of Pgl. In andesite intruded by the Pgl stock, propyritic zones are commonly distributed , while the phyllic zone is present close to Pgl. The potassic zone is characterized by the presence of a small amount of potassic feldspar and many anhydrites, the phylitic zone mostly by $2M_1$ type sericite, and the propyritic zone by many magnetites. The alteration pattern of this survey area resembles the pattern of the Ulutas porphyry copper type ore deposit. A neighbour of this survey area, it lacks potassic feldspar and biotitization of hornblende exists in mineralized granodioritic porphyry(Taylor and Fryer, 1980).

As a result of the discovey of the promising anomalous area of Cu and Mo, three drill holes, totaling 1,003 m in length, were carried out to explore this mineralized area which was expected to be emplaced underground. These three holes discovered a copper and molybdenum mineralized zone, although grade of Cu and Mo varies. The grade of Cu and Mo improved successuvely from MJT-1 to MJT-2 to MJT-3; 0.091 % of mean equivalent Cu in MJT-1 (9.90 m ~ 301.00 m), 0.257 % in MJT-2 (9.50 m ~ 301.00 m) and 0.345 % in MJT-3 (0.00 m ~ 401.00 m). the highest grades for Au(60 ppb), Sn(2ppm) and W(17 ppm) were also obtained, but gold content is lower than expected.

Fracture pattern is an important guide to explore the mineralized zone, for example, in the planning of drilling inclination. Geological and core logging surveys were performed marking the regularity of fracture patterns in the intrusuve rock (Pgl) and in the andesite intruded by Pgl. However, the survey could not define any regurality of fracture patterns in the rocks.

Mineralization paragenesis are mostly pyrite-quartz, pyrite-molybdenite-quartz, chalcopyrite-pyrite, and chalcopyrite-pyrite-quartz, all embedded along fissures. Mineralization in MJT-1 and MJT-2 are emplaced along fissures, while disseminated mineralization is mainly in MJT-3. Predominant dissemination in MJT-3 results in a higher grade of Cu and Mo in compararison with grades of MJT-1 and MJT-2.

Fluid inclusions are mostly gaseous and liquid phases smaller than 10 μ in size. Polyphase inclusions are included in very small amounts considering that it is a porphyry type ore deposit. Solid materials in the inclusions are mostly halite. Rock intruded contains a very small amount of gaseous inclusions. On the other hand, the potassic zone of altered porphyritic granite distributed around the area from Mat Stream to Hasan Stream contains a large quantity of gaseous inclusions, and their homogenizatiom temperatures are higher compared with inclusions of other areas. Around that area, solid inclusions predominantly occur, and the co-existence of dense fluid inclusions (polyphase) and thin fluid inclusions (gaseous phase) reveals that it might have been boiling condition at the formation time of these inclusions.

Geophysical survey (SIP method) carried out using drilling holes obtained PFE anomalies in the area of strong pyrite-mineralization, and distinguished the non- mineralization part bounded by the fault. The data obtained is very effective for further exploration work of the mineralization.

2 Conclusion of the Karadağ Area

Skarn stratum was precedently formed in the boundary between the massive limestone stratum and the underlying basaltic andesite- its pyroclastic rock of A1 Member (Zigana Formation), and granodiorite and quartz porphyry stocks have intruded along the NE~SW striking fault in and adjacent to be area of the skarn strutum. Disseminated mineral showings containing copper or copper-zinc of the Karadağ Area are embedded in the skarn and the stocks. Garnet and epidote are main skarn minerals in the mineral showing, but the amounts of specularite and magnetite are very small compared to similar ore deposits including the Belen Tepe ore deposit at a near locality. In the old Karadağ mine site, chalcopyrite and sphalerite are observed in outcrops and boulders, but most ores are oxidized and only secondary oxide copper minarals are megascopically visible Cerusite was detected by X-ray diffraction analysis. Chemical assay of chipped samples revealed

that the many ore samples contained considerable zinc and copper in the order of 10 %. Such an oxidized copper zone can be traced over one km along the N-S striking limestone. This limstone stratum is displaced by a fault in the central part of the survey area. The copper-lead-zinc mineralized zone is distributed on the north side of the fault, while the copper zone is on the south side of the fault, indicated by result of chemical assay .

Semi-detailed geological survey and geophysical survey (SIP and conventional IP methods) were performed in the promising ore deposit area extending into limestone, andesite and intrusive stock. As a result, three promising anomalous zones were selected. These anomalous zone were detected as PFE anomalies first by conventional IP survey. Detailed SIP method was performed on these PFE anomalies. The survey result indicates that a promising primary mineralized zone may be present in a deeper zone.

3 Recommendation for the Third Phase

It is recommended that the following works are conducted at the most promising areas mentioned above.

(1) the Hasandere Area : Geological, geophysical (SIP method) and drilling surveys of this phase indicate that a promising porphyry copper type ore deposit is expected to be emplaced at the area centered at Mat and Hasan Deres.

Drilling survey reveals that mineralization improves in grade of ore from MJT-1 to MJT-2 to MJT-3. Secondary enrichment occurs, even though it is thin, and the mean value of is 0.345 % equivalent copper grade, (the highest grade among the three drill holes), ranges from surface to hole bottom (401m) in MJT-3. It is expected that this mineralization will prove to be minable as a result of future drilling surveys. It is recommended that drilling survey be performed around MJT-3 to reveal where the high copper grade ore deposit extends to, and that SIP survey also is also carried out to trace the extension of the mineralization.

(2) the Karadağ Area : Three anomalous areas regarded as mineralization were found by the geophysical surveys (SIP and conventional IP methods) in the second phase. In the area, an inferred fault striking NE~SW was interpreted through geological surveys, and intrusive rocks have intruded in the structurally, weak zone, accompanying by mineralization. It is recommended

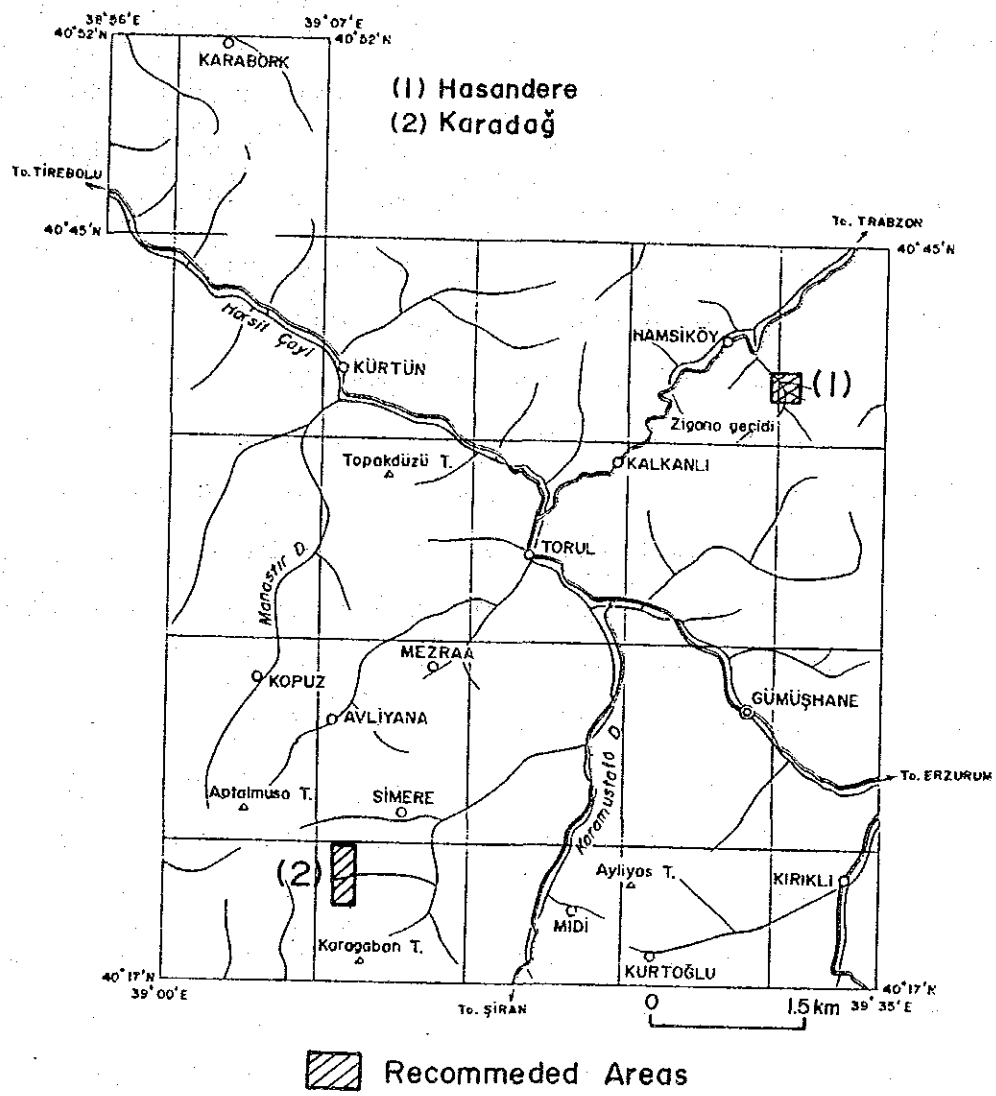

Fig.84 Planning Map Recommended for the Third Phase

for further explorations that drilling survey be carried out to confirm an ore deposit in the expected mineralized area.

REFERENCES

【Geology References】

Akıncı,Ö.T.(1985) : The Eastern Pontide volcano-sedimentary belt and associated massive sulfide deposits. Special publication of the Geological Socicty No.17 , Dixon.E. and Robertson, A.H .F. (Eds.) Blackwell Scientific Publication. Oxford.

Bateman,P.C. et al (1963) : Professional Paper 414-D, U.S. Geological Survey

Blackie (1985) : A Practical Guide to Fluid Inclusion, Chapman and Hall, New York

Bloom,H (1966) : Geochemical Exploration as Applied to Copper-Molybdenum Deposits

Charles,S.N (1976) : *Porphyry Deposits of the Canadian Cordillera. CIM, Special Volume 15*

Chappell,B.W. and White,A.T.R.(1974) : Two contrasting granite types. Pacific Geol. 8, 173-174

Coolbaugh,D.F.(1979) : Geophysics and geochemistry in the disicovery and development of the La Caridad porphyry copper deposit, Sonora,Mexico. Geophysics and Geochemistry in the Search for Metallic Ore.Edited by D.J.Hood

D'Andria,I.(1940) : Gümüşhane kurşun Yatağı hakkında muhtıra.Derl. No.999

Delaloye,M.,Çoğulu,E. and Chessex,R.(1972) : C.R. des Seances , SPHN Geneve 7,43-52

Dixon,C.J. and Pereira,J.(1974) : Plate tectonics and mineralization in the Tethyan region. Mineral. Deposita, 9, 185-198.

Gattinger,T.E.,Erentöz,C. and Ketin, I.(1962) : Explanatory text of the geological map of Turkey, Trabzon,1: 500,000 ,MTA

Ishihara,S.(1977) :*The magnetite-series and ilmenite-series granitic rocks. Mining Geology*, 27, 293 -305.

Ishihara,S. and Takenouchi,S. eds.(1980) : Granitic Magmatism and Related Mineralization. Mining Geology Special Issue,No.8, Soc.Min.Geol.of Japan, p.247

JCPDS(1980) : Mineral powder diffraction file, Data Book, International Center for Diffraction Data.

Kamitani,M. and Akinci,O.T.(1979) : Alpine granitoids and related tungsten-molybdenum deposits in Turkey. Mining Geology,29, 341-350.

Kovenko,V.(1937) : Gumushane madeni hakkinda rapor. Derl. No.399.

Lemmlen,G.G.and Klevtsov,P.V.(1961) : Relations among the principal thermodynamic parameters in a part of the system H2o-NaCl. Geochemistry,No 2,148~158

Lepeltier,C.(1969) : Simplified statistical treatment of geochemical data by graphical representation. Econ.Geol. 64, 538-550.

Mason,B.(1966) : Principle of Geochemistry(Third Edition), Johm Wiley & Sons, Inc. New York.

Nagano,K. et al (1977) : Fluid Inclusion Study og the Mamut Porphyry Copper Deposit,Sabah, Malaysia. Mining Geoligy,27, 201~212

Nash,J.T.(1967) : Fluid-Inclusion Petrology Data from Porphyry Copper Deposits and Applications to Exploration. Geological Survey Professional Paper 907-D

Sannon,JR.S.S.(1971) : Evaluation of Copper and Molybdenum Geochemical Anomalies at the Cumo Prospect,Boise County Idaho. CIM, Special Volume 11

Sillitoe,R.H., Jaramillo,L. and Castro,H.(1984) : Geologic exploration of a molybdenum-rich porphyry copper deposit at Mocoa, Colombia. Econ.Geol. 79, 106-123. Taylor,R.P.and Fryer,B.J.:Multiple-Stage Hydrothermal Alteration in Porphyry Copper system in Northern Turkey . Can. J. Earth Sci. Volume 17 ,1980

Takenouchi,S.(1962) : Polyphase Inclusions in the Quartz from the Taishu Mine. Mining Geology, Vol.12, No.55

(1978) : Fluid Inclusions and Ore-forming Fluids of Porphyry. Mining Geology Vol. 28, No.148

Titley,S.R. and Hicks,C.L.eds.(1966) : Geology of the Porphyry Copper Deposits,South- western North America. Tucson,Univ.Arizona Press, p287.

Titley,S.R. and Beane,R.E.(1981) : Porphyry copper deposits. Economic Geology 75th anniversary Volume,214-269.

Titley,S.R.eds.(1982) : Advances in Geology of the Porphyry Copper Deposits South western North America.Tucson, Univ. Arizona Press.

Turkish-Japan Joint Project(1977) : Consolidated Report on Geological Survey of Trabzon area, Northeastern Turkey. Metal Mining Agency of Japan.

Watanabe,M., Shimada,N. and Yoshida,T. : Fluid inclusion study on the granitic rock and possibly related ore deposits in the Tsumo mining district, southwest Japan. Mining Geology Special Ed. No.9, P. 145~162

Waterman,G.C. and Hamilton,R. L.(1975) : The Sar Cheshmeh Porphyry Copper Deposit.Econ. Geol. 70, 568-576.

White,W.H., et al(1981) : Character and Origin of Climax-type Molybednum Deposits.Econ.Geology 75th Anniversary Volume,270-316.

Yilmaz,Y.(1974) : Geolgy of the Gumushane Granite(Petrography). Istanbul Univ. Fen Fac.Mec. Seri B 39,157-172.

【SIP References】

Dey,A.and Morison,H.F.(1973) : Electromagnetic coupling in frequency and time-domain induced-polarization surveys over multilayered earth,Geophysics,Vol.38,P.380-405.

Hohmann,G.W.(1973) : Electromagnetic coupling between grounded wires at the sur-face of a two layered earth,Geophysics,Vol.38,P.854-863

Pelton,W.H.,Ward,.S.H., Hallof, P.G. ,Sill,W.R., and Nelson,P.H.(1978) :

Mineral discrimination and removal of inductive coupling with Multifre-quency IP,Geophysics ,Vol. 43,P.598-609

Hallof,P.G.and Pelton,W.H.(1980) :The removal of inductive coupling effects from spectral IP data,.S.E.G.50th Annual International Meeting in Houston

Hallof P.G. and Klein,J.D.(1982) : Electrical parameters of volcanogenic mineraldeposits,.S.E.G.52 nd Annual International Meeting

Apêndices

Measurement List of Fluid Inclusion

Sample No	V/P	Name and Description	Homogeniza.T.		Salinity	
	V/P		Pcs	Average	Pcs	Average
AE- 7	V	Qz-vein in andesite	21	409	4	8.7
AE- 8	V	Qz-vein in pgl	16	308	3	5.8
AE- 8	P	Qz-phenocryst of pgl	13	342	2	7.2
AE- 9	P	Qz-pheno,pgl	13	321	2	10.7
AE-11	P	Qz-pheno of pgl	20	382	3	9.2
AE-13	P	Qz-pheno of pgl	10	321	2	6.3
AE-15	V	Py-Qz vein in andesite	20	366	3	8.7
AE-16	V	Py-Qz vein andesite	19	381	3	6.9
AE-18	V	Py-Qz vein in andesite	15	369	*	*
AE-23	V-1	Py-Qz vein andesite	14	362	3	10.8
AE-23	V-2	Mo-Py-Qz vein in andesite	17	349	3	9.2
AE-24	V	Mo-rich Py-Qz vein in and.	20	340	3	7.5
AE-25	V	Mo-rich Py-Qz vein in and.	18	396	3	12.4
AE-31	V	Mo-Py-Qz vein in sili and.	15	381	2	10.8
AE-33	V	Mo-Py-Qz vein in sili and.	14	339	2	7.2
AE-37	V	Py-(Mo)-Qz vein in sili and.	17	391	3	14.3
AE-39	V	Py-Mo-Cp-Cc?-Qz vein in and.	12	342	3	17.7
AE-42	V	(Py)-Qz vein in andesite	10	350	3	12.9
AE-43	V	Qz-vein in sili-ser pgl	20	401	3	16.5
AE-45	P	Qz-phenocryst of pgl	15	328	2	9.8
AE-54	P	Unaltered pg2	20	362	4	12.2
AE-56	P	Unaltered pg2	20	362	*	*
YY- 5	V	Mo-Qz vein in andesite	22	404	3	11.7
YY- 6	P	Qz-pheno of pgl	16	377	3	7.5
YY- 9	V	(Py)-Qz vein of pgl	18	361	4	14.1
YY-12	P	Qz-pheno of unaltered pgl	14	477	3	17.5
YY-15	V	Py-Qz-vein of pgl	20	408	3	15.4
YY-15	P	Qz-pheno of pgl	12	361	2	11.8
YY-18	P	Qz-pheno of pgl	16	347	3	14.3
YY-33	P	Unaltered pg2	20	333	*	*

Sample No	V/P	Name and Description	Homogeniza.T		Salinity	
			Pcs	Average	Pcs	Average
YY-26	V	Py-Qz vein pgl	15	366	4	14.4
YY-26	P	Qz-pheno of pgl	13	352	3	17.2
YY-27	V	Py-Qz vein of pgl	20	405	4	17.1
YY-27	P	Qz-pheno of pgl	18	403	3	17.2
YY-29	P	Qz-pheno of pgl	15	396	3	19.5
HY- 1	V	Mo-Qz vein in andesite	20	351	3	11.0
HH- 9	V	Pgl with Mo.Py,Qz,vein	20	384	4	8.5
HH-13	P	Qz-pheno of pgl,Py-diss	16	385	2	9.9
HH-19	P	Qz-pheno of wht-alt pgl	17	304	3	9.2
HH-21	P	Pgl with Py diss	15	304	3	12.2
HH-24	V	Qz-vein of biotite-alt pgl	20	391	3	12.2
HH-24	P	Qz-pheno of biotite-alt pgl	20	510	*	*
HH-27	V	Qz-vein of alt pgl	20	364	4	8.5
HH-36	P	Qz-pheno of greenish pg2	21	344	3	12.2
HH-37	P	Qz-pheno of gry glassy pg2	17	314	*	*
HH-46	P	Qz-vein wht pgl	20	415	*	*
HH-46	V	ditto	20	408	3	17.2
HH-47	V	Qz-veinlets of pgl	18	354	4	17.1
HH-53	V	Qz-veinlets of pgl	20	357	3	8.1
HH-53	P	Qz-pheno of sili-limo.pgl	12	400	3	10.5
KY- 1	V	Py-Qz vein in andesite	20	386	3	12.2
KY- 9	V	Py-Qz vein in andesite	20	345	3	10.5
KY-12	V	Mag-Py-Qz vein in andesite	20	361	4	10.3
KY-18	V	Mo-Py-Qz vein in andesite	15	453	*	*
KY-19	V	Mo-Py-Qz vein of pgl	15	386	3	15.4
KY-19	P	Qz-pheno of pgl	20	397	3	17.7
KY-20	P	Qz-pheno of pgl	20	406	4	12.2
KY-21	V	Mo-Qz vein of pgl	20	390	4	18.0
KY-21	P	Qz-pheno of pgl	18	383	4	13.1
KY-23	V	Mo-Qz vein of pgl	20	389	3	12.4
KY-24	V	Mo-Qz vein of biotite pgl	17	399	*	*
KY-24	P	Qz-pheno of biotite pgl	17	461	3	20.1
KY-25	P	Pg with Mo-Qz vein	17	413	4	15.8
KY-25	V	Pg with Mo-Qz vein	16	479	3	19.3
KM- 4	V	Qz-veinlets of pgl	10	467	2	17.9
KM-21	V	Qz-vein(float) from andesite	20	404	4	14.4
KM-25	V	Qz-vein of andesite	17	403	*	*

MJT-1 No 3

Depth(m)	V/P	Name and Description	Homoginiza.T		Salinity	
			Pcs	Average	Pcs	Average
52.8	V	Py-Cp-Qz vein in andesite	20	385	*	*
99.8	V	Py-Mo-Cp vein in andesite	20	375	*	*
138.0	V	Py-Mo-Qz vein in pgl	20	406	3	17.2
183.3	V	(Mo-Py)-Qz vein in pgl	20	378	*	*
183.3	P	ditto	15	349	2	12.6
210.5	V	Magnetite-Py-Qz vein in and.	15	392	*	*
222.8	V	Py-Cp-Mo-Qz vein in and.	20	401	4	17.7
290.7	V	Mo-Py-Qz vein in and.	15	420	*	*

MJT-2 No 4

Depth(m)	V/P	Name and Description	Homoginiza.T		Salinity	
			Pcs	Average	Pcs	Average
58.4	V	Mo-Qz vein in andesite	12	365	*	*
68.5	V	Cp-Qz vein in andesite	12	371	*	*
71.8	V	Cp-Mo-Qz vein in andesite	15	393	*	*
129.8	V	Qz vein in andesite	20	383	*	*
145.3	V	Magnetite-Cp-Qz vein in and.	20	398	4	17.1
213.5	V	Mo-Qz vein in and.	20	371	*	*
248.0	V	Mo-Qz vein in and	20	406	4	14.4
255.3	V	Py-Mo-Qz vein in and	15	357	3	12.9
268.5	V	Magnetite-Cp-Qz vein in and.	20	409	4	15.0
272.9	V	Mo-Qz vein in and.	20	401	3	17.2
278.0	P	Porphyritic granite(pgl)	10	387	*	*
283.4	V	Py-Cp-Qz vein in and.	20	410	*	*

MJT- 3 No 5

Depth(m)	V/P	Name and Description	Homoginiza.T		Salinity	
			Pcs	Average	Pcs	Average
10.15	P	Qz-pheno of pgl	15	404	4	13.8
59.0	V	Cp-(Mo)-Py-Qz vein	18	409	4	16.0
59.0	P	ditto	15	384	*	*
80.3	V	(Mo)-Py-Qz vein in pgl	18	399	3	12.9
118.7	V	Mo-Qz vein in pgl	10	440	2	11.8
196.0	V	Cp-Py vein in pgl	20	428	4	16.8
238.9	P	Pgl with disseminated Cp-Py.	20	397	3	17.9
255.6	P	Pl-rich pgl	17	435	4	15.5
258.0	A	Qz-anhydrite vein in pgl	15	416	*	*
312.5	P	Qz porphyry	15	422	3	17.9
328.1	P	Qz porphyry with Cp-Py diss.	20	409	4	15.5
378.0	V	Py-Mo-Qz vein in pgl	10	409	*	*
400.6	P	Qz porphyry with Cp-Py diss.	20	435	4	14.4

Homoginiza.T ; Homoginization Temperecture (℃)

Salinity ; NaCl wt %

* ; Impossible to Measure Salinity of Fluid Inclusion

Hasandere Area

Phase spectra and Cole-Cole diagrams
of Rock Samples

Sample No. 1

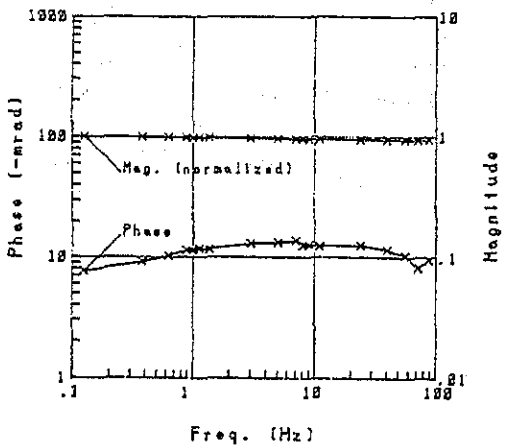

Sample No. 2

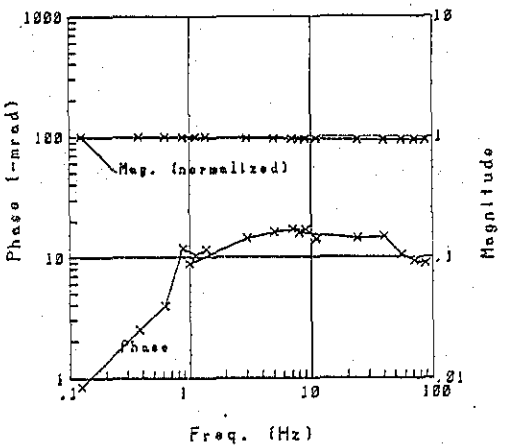

Sample No. 3

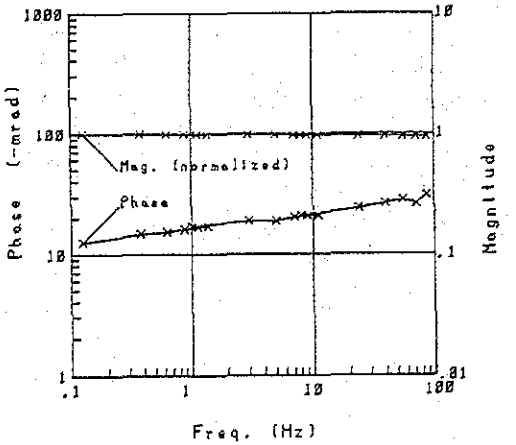

NO. 1 Cole-Cole Diagram

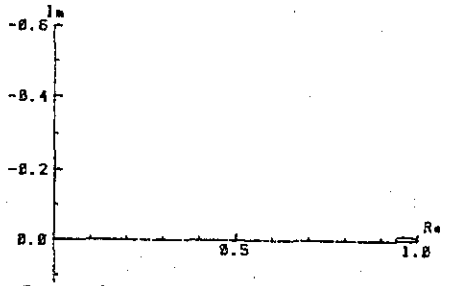

Rock	: Andesite	
Spectrum	: X	type
Phase	: 7.6	-mrad
P F E	: 1.22	%
Resistivity	: 639	ohm-m

NO. 2 Cole-Cole Diagram

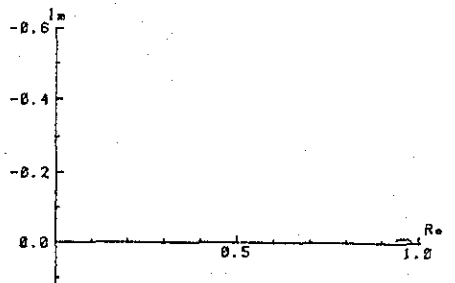

Rock	: Andesite	
Spectrum	: D	type
Phase	: 0.8	-mrad
P F E	: 0.09	%
Resistivity	: 290	ohm-m

NO. 3 Cole-Cole Diagram

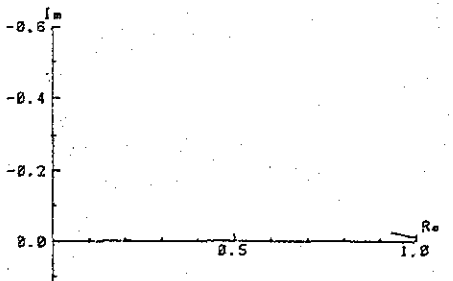

Rock	: Andesite	
Spectrum	: A	type
Phase	: 12.6	-mrad
P F E	: 1.94	%
Resistivity	: 2,236	ohm-m

Sample No. 4

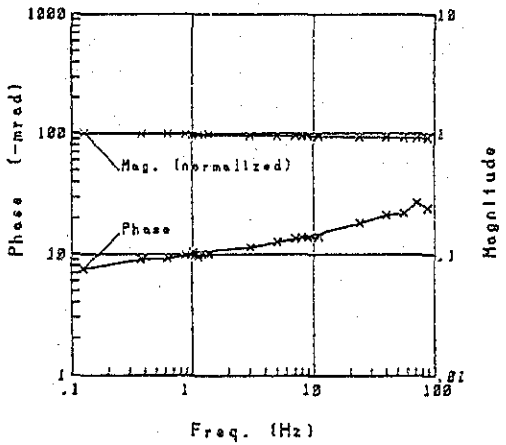

Sample No. 5

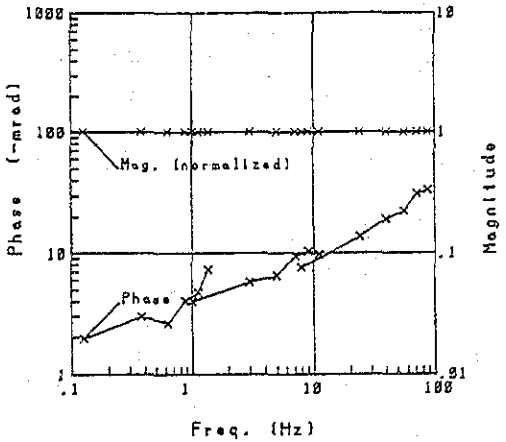

Sample No. 6

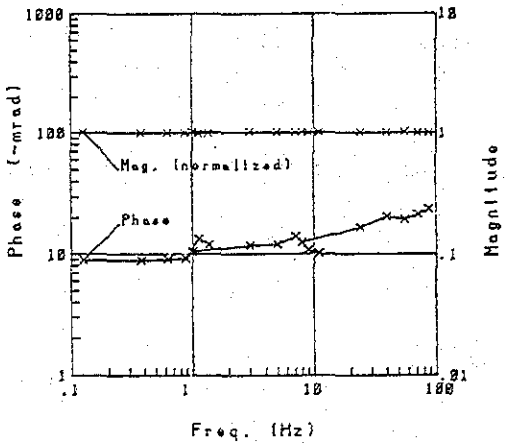

NO. 4 Cole-Cole Diagram

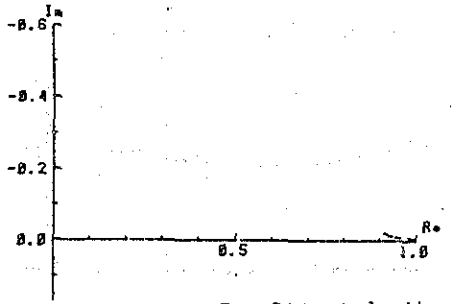

R o c k	: Basaltic Andesite	
Spectrum	: A	type
Phase	: 7.5	-mrad
P F E	: 1.22	%
Resistivity	: 7,164	ohm-m

NO. 5 Cole-Cole Diagram

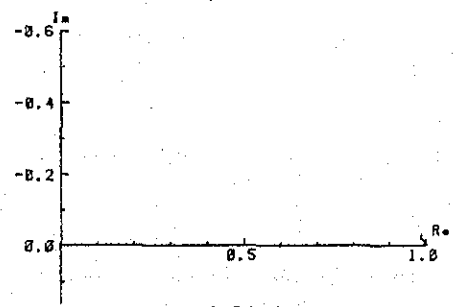

R o c k	: Siltstone	
Spectrum	: A	type
Phase	: 1.9	-mrad
P F E	: 0.32	%
Resistivity	: 12,649	ohm-m

NO. 6 Cole-Cole Diagram

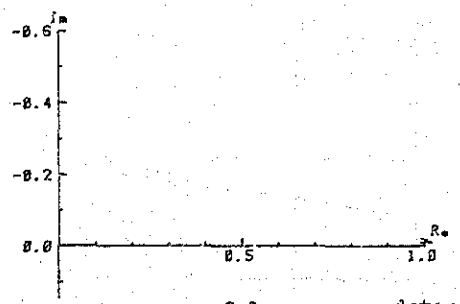

R o c k	: Calcareous mudstone	
Spectrum	: C	type
Phase	: 10.1	-mrad
P F E	: 1.16	%
Resistivity	: 4,322	ohm-m

Sample No. 7

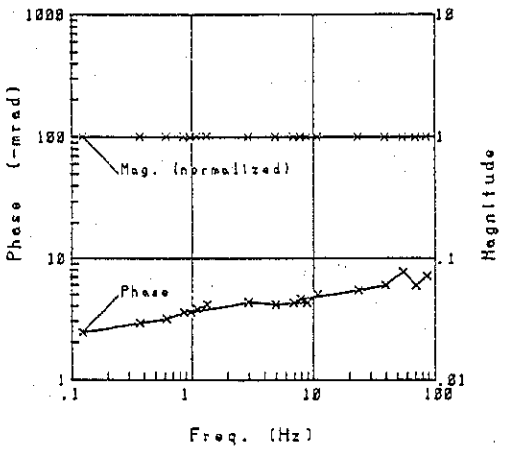

NO. 7 Cole-Cole Diagram

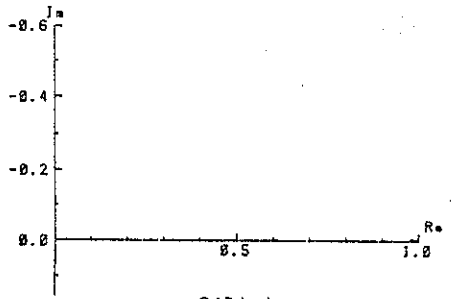

R o c k	: Siltstone	
Spectrum	: A	type
Phase	: 2.4	-mrad
P F E	: 0.34	%
Resistivity	: 3,273	ohm-m

Sample No. 8

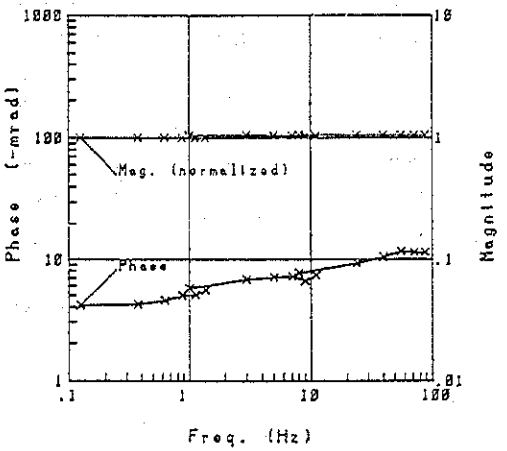

NO. 8 Cole-Cole Diagram

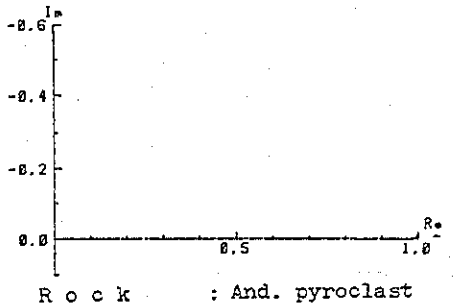

R o c k	: And. pyroclast	
Spectrum	: A	type
Phase	: 4.1	-mrad
P F E	: 0.59	%
Resistivity	: 4,996	ohm-m

Sample No. 9

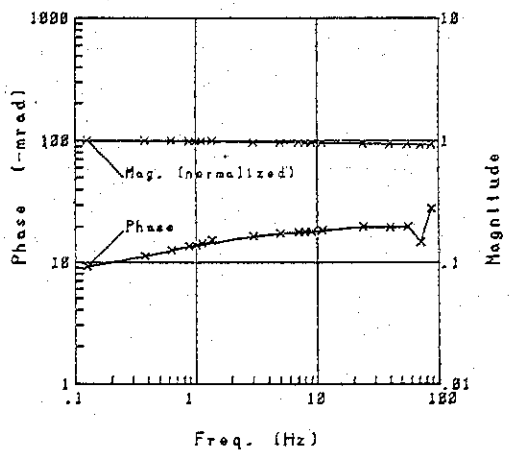

NO. 9 Cole-Cole Diagram

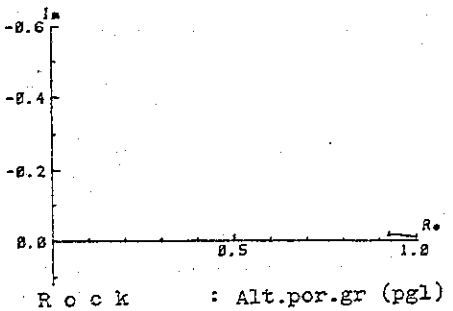

R o c k	: Alt.por.gr (pgl)	
Spectrum	: A	type
Phase	: 9.2	-mrad
P F E	: 1.48	%
Resistivity	: 3,846	ohm-m

Sample No. 10

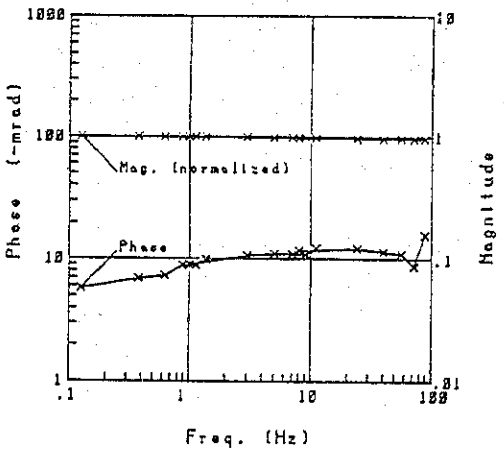

Sample No. 11

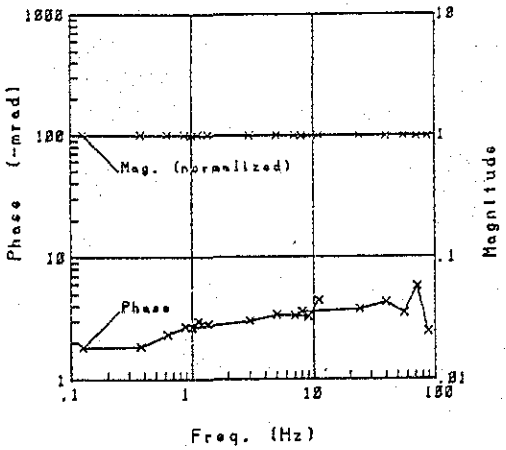

Sample No. 12

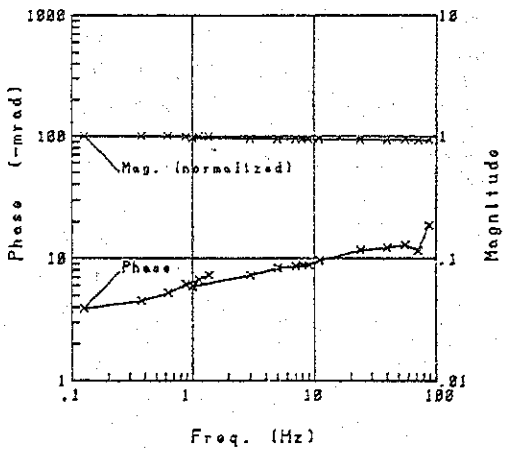

NO. 10 Cole-Cole Diagram

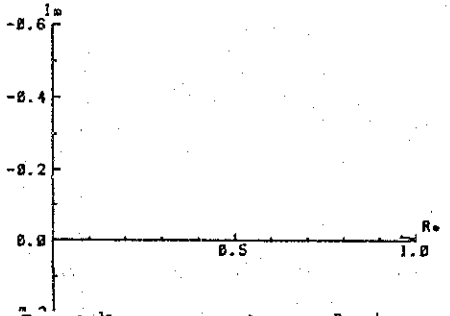

Rock	: And.pyroclast	
Spectrum	: A	type
Phase	: 5.1	-mrad
P F E	: 0.73	%
Resistivity	: 1.819	ohm-m

NO. 11 Cole-Cole Diagram

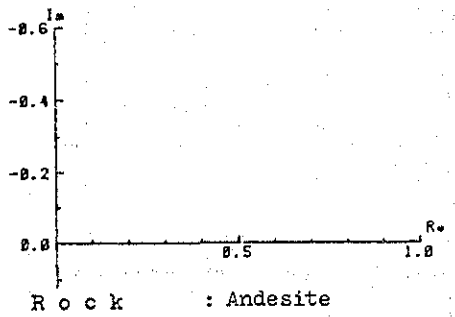

Rock	: Andesite	
Spectrum	: A	type
Phase	: 1.4	-mrad
P F E	: 0.19	%
Resistivity	: 2,544	ohm-m

NO. 12 Cole-Cole Diagram

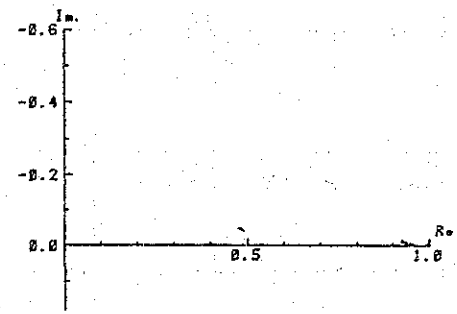

Rock	: And.pyroclast	
Spectrum	: A	type
Phase	: 3.9	-mrad
P F E	: 0.58	%
Resistivity	: 4,669	ohm-m

Sample No. 13

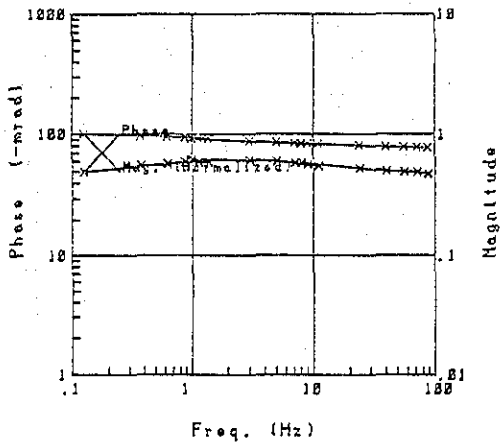

NO. 13 Cole-Cole Diagram

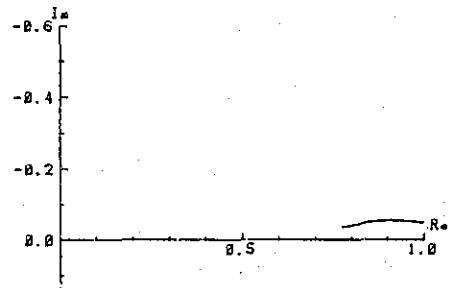

R o c k	: Andesite	
Spectrum	: X	type
Phase	: 49.3	-mrad
P F E	: 7.92	%
Resistivity	: 1,579	ohm-m

Sample No. 14

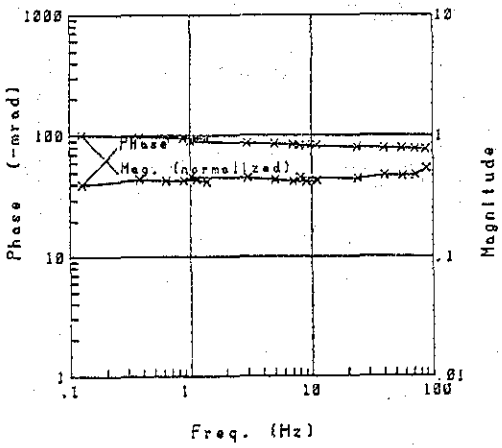

NO. 14 Cole-Cole Diagram

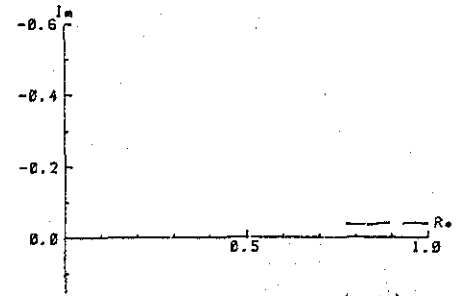

R o c k	: Alt.por.gr (pgl)	
Spectrum	: A	type
Phase	: 4o.o	-mrad
P F E	: 6.19	%
Resistivity	: 7,041	ohm-m

Sample No. 15

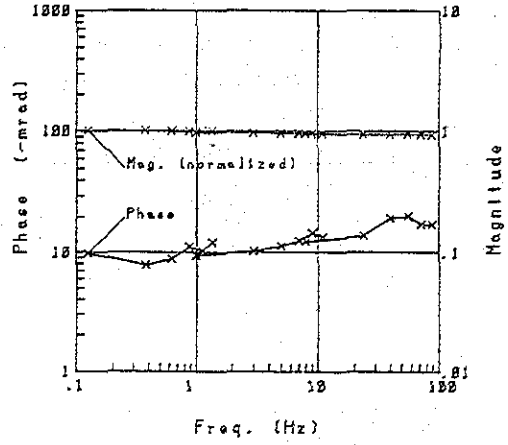

NO. 15 Cole-Cole Diagram

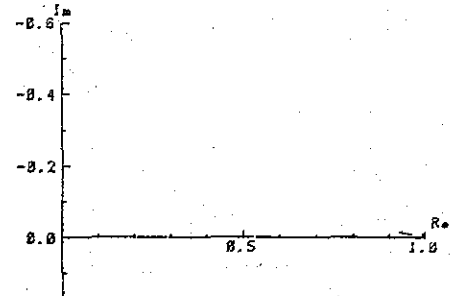

R o c k	: Quartz porphyry	
Spectrum	: C	type
Phase	: 6.5	-mrad
P F E	: 0.84	%
Resistivity	: 5,207	ohm-m

Sample No. 16

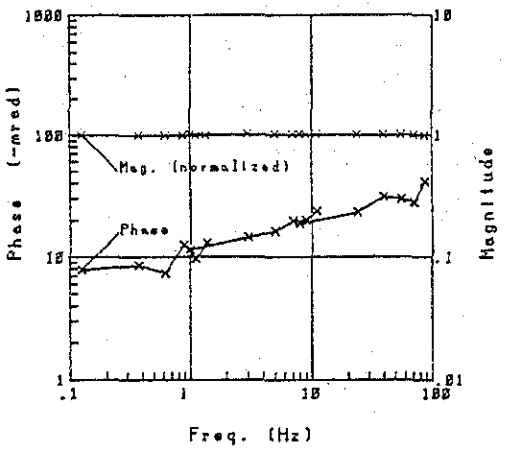

Sample No. 21

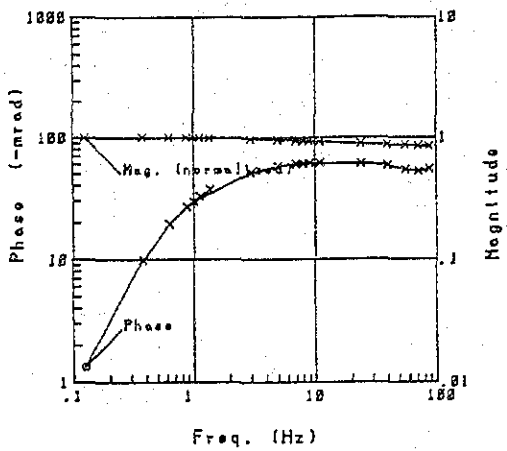

Sample No. 22

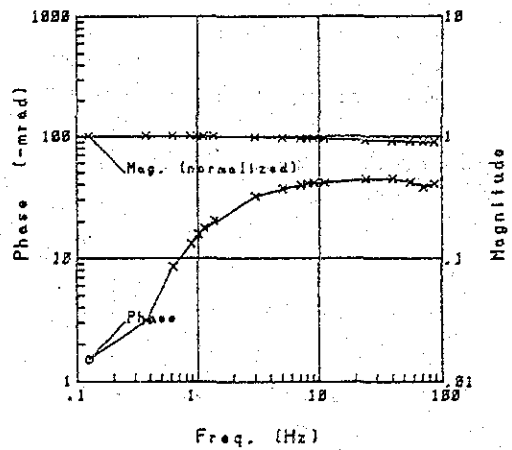

NO. 16 Cole-Cole Diagram

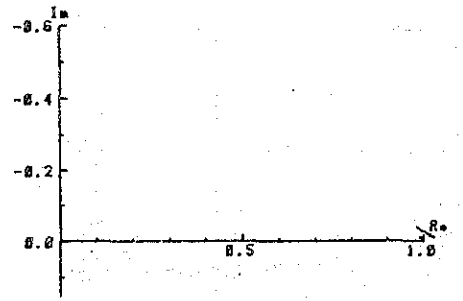

R o c k	: Porphyritic granite (pg2)	
Spectrum	: A	type
Phase	: 7.8	-mrad
P F E	: 0.88	%
Resistivity	: 6,551	ohm-m

NO. 21 Cole-Cole Diagram

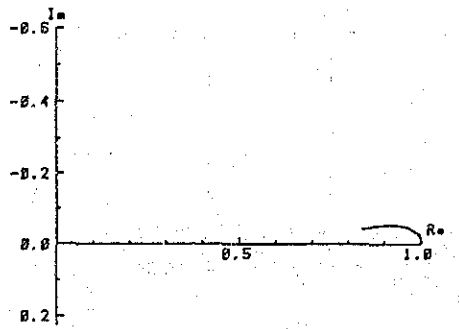

R o c k	: Andesite	
Spectrum	: D	type
Phase	: -2.2	-mrad
P F E	: 0.50	%
Resistivity	: 162	ohm-m

NO. 22 Cole-Cole Diagram

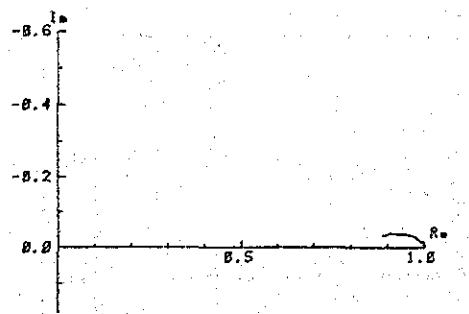

R o c k	: Andesite	
Spectrum	: D	type
Phase	: -4.3	-mrad
P F E	: -0.19	%
Resistivity	: 126	ohm-m

288

Sample No. 23

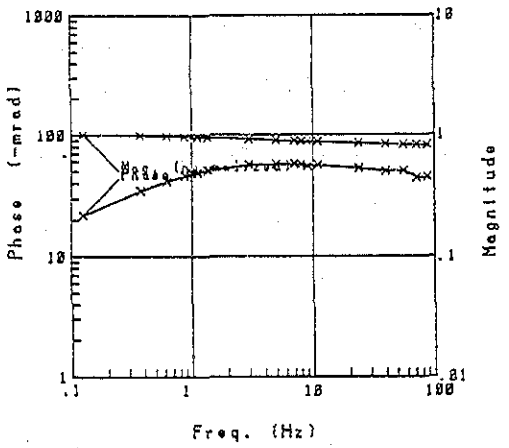

NO. 23 Cole-Cole Diagram

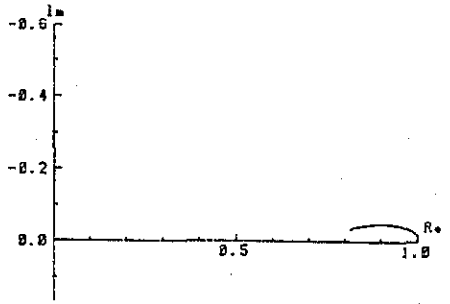

R o c k	:	Alt.por.gr (pgl)	
Spectrum	:	D	type
Phase	:	21.8	-mrad
P F E	:	4.56	%
Resistivity	:	219	ohm-m

Sample No. 24

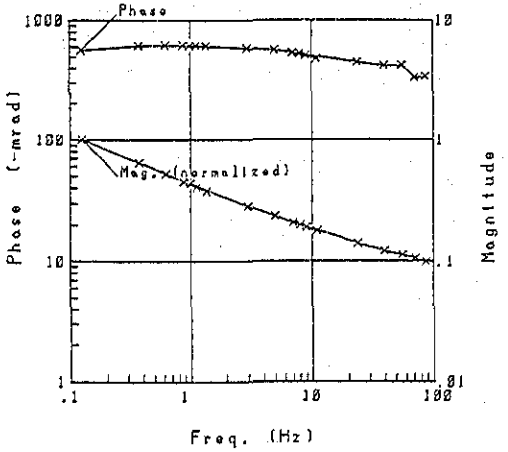

NO. 24 Cole-Cole Diagram

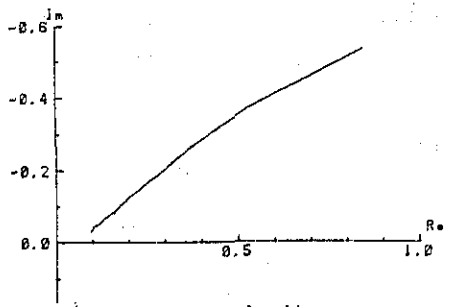

R o c k	:	Andesite	
Spectrum	:	Y	type
Phase	:	561.6	-mrad
P F E	:	134.17	%
Resistivity	:	449	ohm-m

Sample No. 25

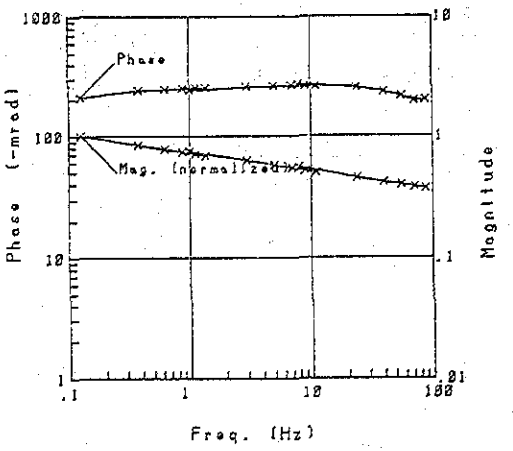

NO. 25 Cole-Cole Diagram

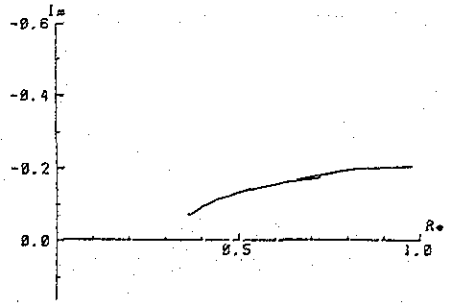

R o c k	:	Alt.por.gr (pgl)	
Spectrum	:	X	type
Phase	:	208.8	-mrad
P F E	:	38.71	%
Resistivity	:	1,795	ohm-m

Sample No. 26

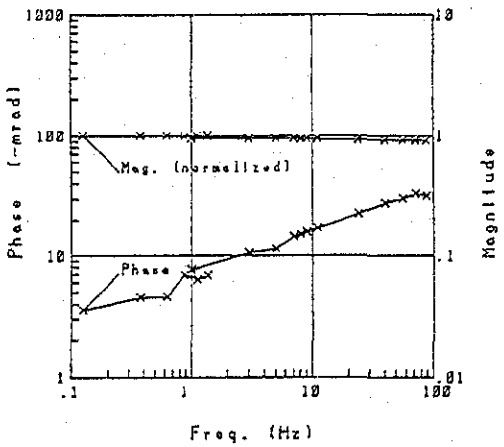

Sample No. 27

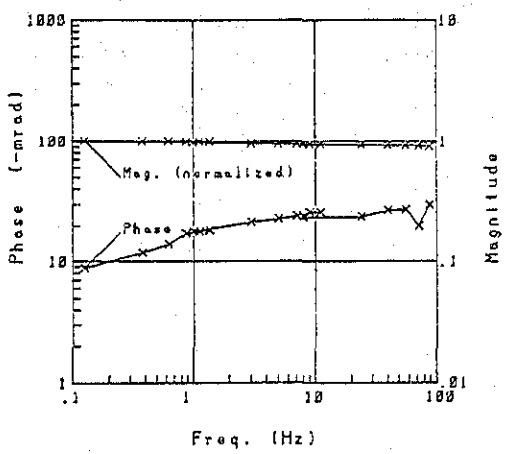

Sample No. 28

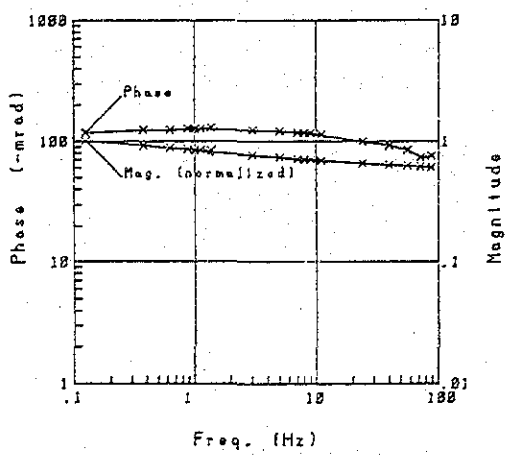

NO. 26 Cole-Cole Diagram

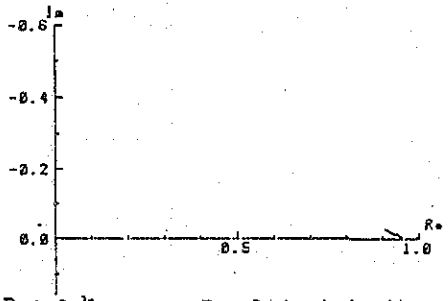

R o c k	: Basaltic Andesite	
Spectrum	: A	type
Phase	: 3.5	-mrad
P F E	: 0.45	%
Resistivity	: 4,757	ohm-m

NO. 27 Cole-Cole Diagram

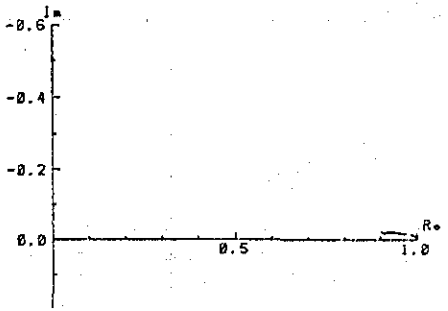

R o c k	: Andesite	
Spectrum	: A	type
Phase	: 8.8	-mrad
P F E	: 1.43	%
Resistivity	: 1.299	ohm-m

NO. 28 Cole-Cole Diagram

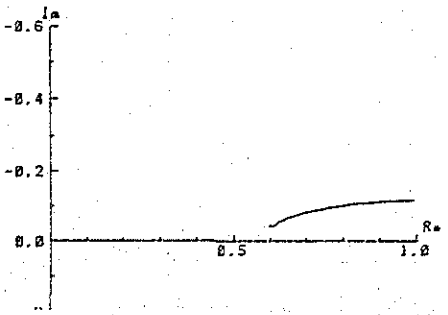

R o c k	: Basaltic Andesite	
Spectrum	: X	type
Phase	: 117.8	-mrad
P F E	: 18.20	%
Resistivity	: 547	ohm-m

Sample No. 29

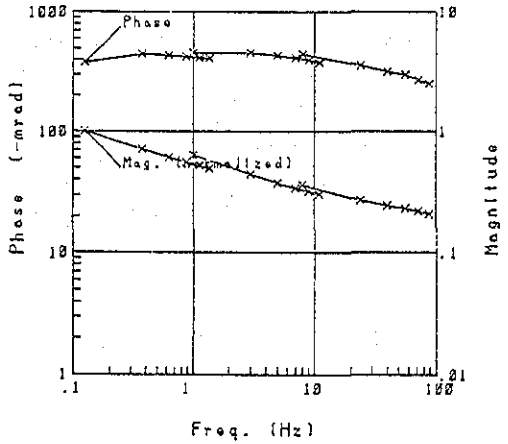

NO. 29 Cole-Cole Diagram

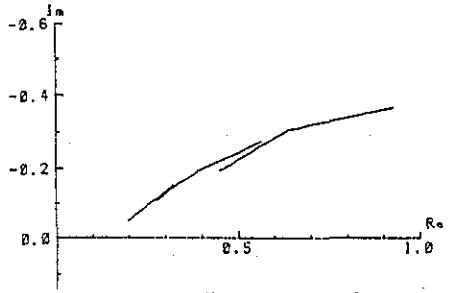

R o c k	:	Basaltic Andesite	
Spectrum	:	X	type
Phase	:	376.2	-mrad
P F E	:	88.31	%
Resistivity	:	1,361	ohm-m

Sample No. 31

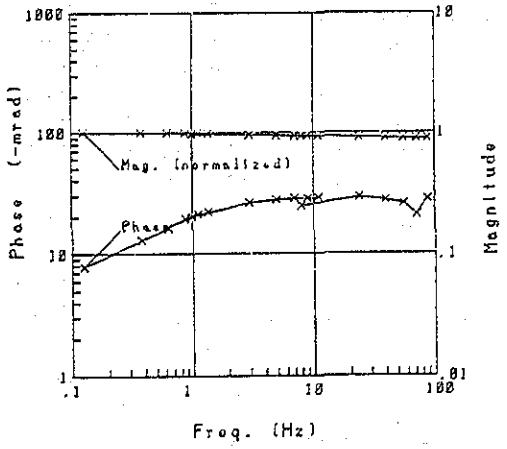

NO. 31 Cole-Cole Diagram

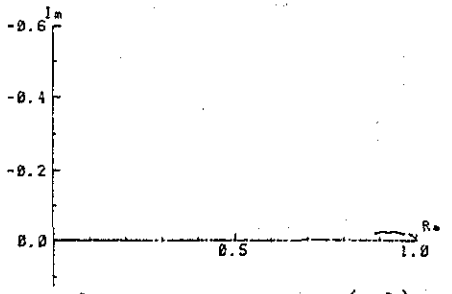

R o c k	:	Alt.por.gr (pgl)	
Spectrum	:	D	type
Phase	:	7.8	-mrad
P F E	:	1.60	%
Resistivity	:	294	ohm-m

Sample No. 32

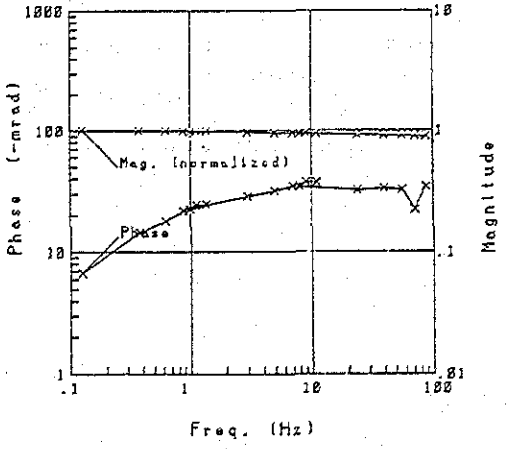

NO. 32 Cole-Cole Diagram

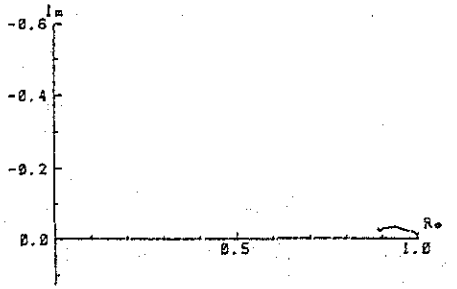

R o c k	:	Andesite	
Spectrum	:	D	type
Phase	:	6.7	-mrad
P F E	:	1.49	%
Resistivity	:	824	ohm-m